https://doi.org/10.5194/egusphere-2026-1788
Preprint. Discussion started: 18 May 2026

Efficient formation of aqueous secondary organic aerosols from the hydroxyl radical reaction with fenchol, borneol, and menthol

Priyanka Jain[1], Bartłomiej Witkowski[1], Agata Błaziak[2], Tomasz Gierczak[1]

[1]Faculty of Chemistry, University of Warsaw, al. Żwirki i Wigury 101, 02-089 Warsaw, Poland
[2]Institute of Physical Chemistry, Polish Academy of Sciences, ul. Kasprzaka 44/52, 01-224 Warsaw, Poland

Correspondence to: Bartłomiej Witkowski (bwitk@chem.uw.edu.pl)

Abstract. Aqueous-phase oxidation of oxygenated monoterpenes can contribute to the formation of secondary organic aerosol (SOA) from biogenic volatile organic compounds. Still, the quantitative and mechanistic data for such precursors are limited. In this study, the aqueous-phase reactions of three atmospherically relevant, saturated terpenoic alcohols (TAs)—fenchol, borneol, and menthol—with hydroxyl radicals (OH) were investigated using a photochemical reactor combined with GC/MS and LC/ToF-MS analyses and kinetic modeling. The objectives were to elucidate reaction mechanisms, identify oxidation products, and quantify yields of aqueous SOA ($_{aq}$SOA) under atmospherically relevant conditions. Comprehensive product analysis revealed that oxidation proceeds via H-atom abstraction, yielding a wide range of multifunctional products. In addition to previously reported products, this work first identified functionalized terpenoic acids formed as second-generation products, providing new evidence for the formation of low-volatility compounds from aqueous OH reaction with TAs. The molar yields of quantified products approached unity (0.88–0.99), indicating near-complete closure of the carbon balance. Based on these data, explicit kinetic box models were developed that successfully reproduced the measured temporal evolution of reactants. Modelled $_{aq}$SOA yields ranged from 10% to 70%, depending on liquid water content and reaction coordinate, representing the first quantitative estimates for the three TAs under investigation. The results demonstrate that aqueous oxidation of semi-volatile terpenoids can efficiently generate low-volatility products contributing to SOA formation. These findings highlight the importance of multiphase processing of oxygenated terpenoids and provide new mechanistic and quantitative data for atmospheric models.

https://doi.org/10.5194/egusphere-2026-1788
Preprint. Discussion started: 18 May 2026

1 Introduction

Fine atmospheric particulate matter (PM) - solid or liquid particles in the air - influences the climate, air quality, and human health (Jo et al., 2023). Aerosols with aerodynamic diameter ≤ 2.5 μm ($PM_{2.5}$) exhibit direct and indirect climate forcing by absorbing and scattering solar radiation, and acting as cloud condensation nuclei (CCN) and ice nuclei (IN), thereby altering cloud albedo and lifespan (Shrivastava et al., 2017a). Furthermore, exposure to $PM_{2.5}$ negatively impacts human health and is associated with various cardiovascular and respiratory conditions, but also with Parkinson's disease, diabetes, etc. (Wei et al., 2019).

Secondary organic aerosols (SOAs) are formed in the atmosphere by oxidation of volatile organic compounds (VOCs) (Chaturvedi et al., 2023; Mahilang et al., 2021). Because about 90% of non-methane VOCs are emitted by vegetation (Sindelarova et al., 2022), the oxidation of these biogenic VOCs (BVOCs) is one of the major sources of SOAs (Mahilang et al., 2021; Shrivastava et al., 2017b). Production of SOAs from BVOCs is currently estimated at 73.6 - 97.5 Tg × yr^{-1}, (Hodzic et al., 2016; Kelly et al., 2018), contributing to up to 90% mass of fine atmospheric PM (Jimenez et al., 2009; Zhang et al., 2005; Xu et al., 2021; Kanakidou et al., 2005).

Isoprene (C_5H_8) is the major BVOC, followed by monoterpenes ($C_{10}H_{16}$), for which the estimated emissions range between 82.7 and 184.8 Tg × yr^{-1} (Wang et al., 2024; Sindelarova et al., 2022). Moreover, the flux of SOAs from atmospheric oxidation of monoterpenes is estimated at ~20 Tg × yr^{-1}, about half of the BSOAs mass (Kelly et al., 2018). Hence, monoterpenoic SOAs significantly contribute to the global budget of fine PM (Jimenez et al., 2009; Fuzzi et al., 2015).

Consequently, the formation of SOAs from the gas-phase oxidation of monoterpenes ($_{gas}$SOAs) was the subject of extensive research for over three decades (Hallquist et al., 2009; Fuzzi et al., 2015). To-date, many studies have focused on the major biogenic monoterpenes: α and β-pinene and limonene (Wang et al., 2024; Sindelarova et al., 2022; Kamens and Jaoui, 2001). Production of SOAs from these BVOCs is initiated primarily by atmospherically abundant oxidants: ozone (O_3), hydroxyl, and nitrate (NO_3) radicals (Mahilang et al., 2021). Oxidation of monoterpenes generates a cascade of oxygenated products, including various water-soluble organic compounds (WSOCs) (Zhang et al., 2015; Kamens and Jaoui, 2001; Kourtchev et al., 2014). The WSOCs contributing to monoterpenoic SOAs include terpenoic acids (TACs), non-acidic monoterpenoids (MTDs), polyfunctional oligomers, many of which are highly oxygenated molecules (HOMs) (Kenseth et al., 2020; Valorso et al., 2011; Yasmeen et al., 2011; Liu et al., 2023). At the same time, the classical model involving the formation of these low-volatility organics followed by their gas-particle partitioning (Pankow, 1994; Odum et al., 1996), does not provide a complete picture of the formation and evolution of SOAs (Su et al., 2020; Carlton et al., 2020; Tsigaridis and Kanakidou, 2018; Ervens, 2015).

Liquid water is ubiquitous in the troposphere, playing a crucial role in the multiphase chemistry of organic and inorganic trace species, including SOAs (Su et al., 2020; Lim et al., 2010; Carlton et al., 2020; Ervens, 2015; Ervens et al., 2018). Consequently, for over a decade, there has been an increasing focus on the still incompletely characterized aqueous reaction in clouds, fogs, haze, and some aerosols in the context of the formation and processing of SOAs (Su et al., 2020; Carlton et

https://doi.org/10.5194/egusphere-2026-1788
Preprint. Discussion started: 18 May 2026

al., 2020; Lim et al., 2010; Ervens, 2015). Reactions of WSOCs in hydrometeors often involve unique species and mechanisms, resulting in HOMs and extremely low-volatility organic compounds (ELVOCs (Ervens, 2015; Zhu et al., 2020; Sullivan et al., 2016; Sun et al., 2010; Ervens et al., 2011; Mekic et al., 2019; Zheng et al., 2021; Gomez et al., 2015). Such molecules can be formed via (photo)chemical and non-radical "dark" reactions, contributing to $_{aq}$SOAs following the evaporation of water (Sullivan et al., 2016; Paglione et al., 2020; Kuang et al., 2020b). Results of field and laboratory studies strongly indicate that the contribution of $_{aq}$SOAs to the total flux of OAs is likely significant, on both global and local scales (Paglione et al., 2020; Kuang et al., 2020b; Su et al., 2020; Tsui et al., 2019). In addition to producing new particles, the multiphase reactions of SOAs also alter physicochemical characteristics of OAs, including composition, optical and toxicological properties, and CNN and IN activity (Carlton et al., 2020; Ervens, 2015; Sullivan et al., 2016; Decesari et al., 2017). At the same time, the fundamental data necessary to parametrize the complex multiphase chemistry of OAs remain incomplete, making it difficult to constrain the climate forcing of fine aerosols (Iccp, 2023; Tsigaridis and Kanakidou, 2018). To-date, many studies have focused on the formation of $_{aq}$SOAs from the reaction of oxygenated terpenoids with OH, because it is a major daytime atmospheric oxidant (Gligorovski et al., 2015). OH is formed by photolysis of O_3 and diffuses into water-containing particles from the gas phase (Price et al., 2025). Additionally, OH is also formed inside hydrometeors by decomposition of hydrogen peroxide (H_2O_2) via photolytic or Fenton(like) processes, enhancing the oxidative capacity of some aqueous particles (Kuang et al., 2020a; Bianco et al., 2020; Scheres Firak et al., 2025).

Studies of $_{aq}$SOAs formation from OH reactions with monoterpenoic precursors have often focused on terpenoic acids and other low-volatility molecules with a high tendency to partition into the aqueous phase (Witkowski et al., 2019; Amorim et al., 2021; Enami and Sakamoto, 2016b; Huang et al., 2018; Otto et al., 2018; Lai et al., 2025). At the same time, the formation of $_{aq}$SOAs from non-acidic MTDs has seldom been investigated, even though such precursors were shown to form HOMs following gas and aqueous oxidation by OH and O_3 (Leviss et al., 2016; Li et al., 2020). Moreover, the measured yields of $_{gas}$SOAs from oxidation of some MTDs were similar or higher than monoterpenes (Khalaj et al., 2025; Griffin et al., 1999).

Our recent study was focused on aqueous OH reactions with two terpenoic diols: pinanediol and camphanediol (Jain et al., 2024). These terpenoids are characterized by dimensionless Henry's law constant values comparable with terpenoic acids ($H^{cc}\approx1\times10^5$) (Episuite4.11). Moreover, the mass yields of SOAs from OH reactions with terpenoic 1,2-diols were close to 100% in both the gas and aqueous phases (Jain et al., 2024; Ye et al., 2018), highlighting the potential of some MTDs to contribute to the ambient, fine PM mass.

The presented work focused on $_{aq}$SOAs formation from aqueous OH reaction with three terpenoic monoalcohols (TAs): fenchol (FCH), borneol (BNL), and menthol (MTH) - Fig. 1. The goals of this work include analyzing products, mechanisms, and $_{aq}$SOAs yields from R1-3.

https://doi.org/10.5194/egusphere-2026-1788
Preprint. Discussion started: 18 May 2026

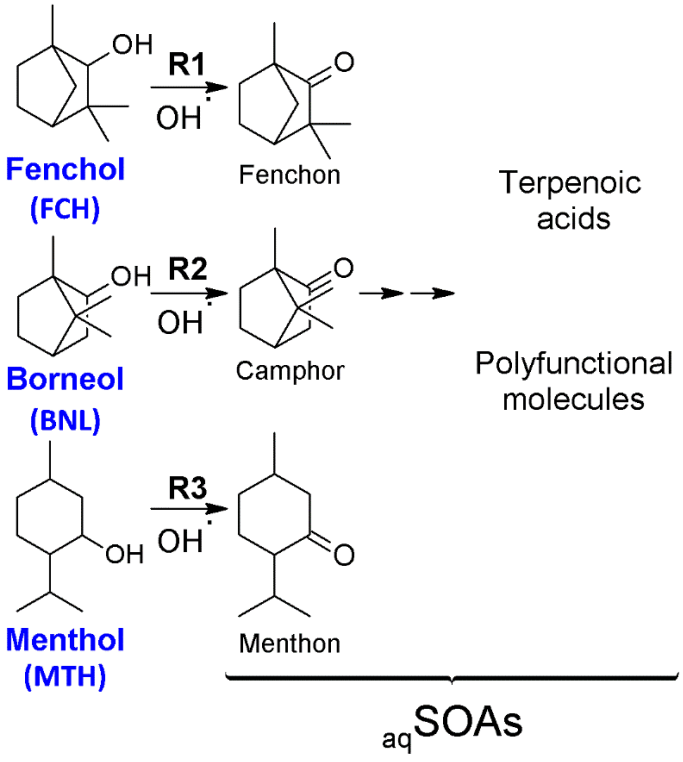

Figure 1: Precursors and reactions investigated.

The TAs under investigation (Fig. 1) are more volatile than terpenoic diols and acids and will likely remain in the gas phase when there is no water present (Keating et al., 2017). At the same time, the TAs are semi-volatile organic compounds (SVOCs) that can enter water particles ($H^{cc} \approx 1 \times 10^3$) under the realistic atmospheric conditions (Mcneill, 2015; Witkowski et al., 2024b). As concluded in our previous study, FCH, BNL, and MTH can react with OH in the aqueous phase in air masses with liquid water content (LWC) ≥ 0.1 g×m^{-3} (Witkowski et al., 2024b).

In addition to secondary formation from monoterpene oxidation (Valorso et al., 2011), the sources of emission of MTDs include wildfires (Hatch et al., 2019) and natural and agricultural vegetation (Messina et al., 2016; Guenther et al., 2012; Gentner et al., 2014; Graedel, 1979). MTDs are emitted by crops, alpines, grasslands, forests, flowering plants, harvesting activities, and due to the use of fertilizers (Ormeño et al., 2010; Gentner et al., 2014; Yang et al., 2021). MTDs also largely contribute to the distinctive fragrances of essential oils and flavors found in plants, resulting in their widespread industrial uses (Caputi and Aprea, 2011; Zuzarte and Salgueiro, 2015).

The three TAs under investigation (Fig. 1) are among the major components of essential oils, emitted by plants, but are also emitted during wildfires (Kamatou et al., 2013; Hatch et al., 2019; Ghaffari et al., 2019; Yassaa et al., 2000). Particularly, MTH has a wide variety of industrial and medical uses, with the estimated annual consumption of about 30 000 metric tonnes (Kamatou et al., 2013). Moreover, FCH and BNL were included in the combined global emissions of 14.9 Tg yr^{-1} for

https://doi.org/10.5194/egusphere-2026-1788
Preprint. Discussion started: 18 May 2026

34 MTDs, compared with 66.1 Tg yr^{-1} estimated for α-pinene (Guenther et al., 2012). Additionally, the total flux of TAs was estimated at 14.6 Tg yr^{-1}, 9% of total monoterpene emission (Griffin et al., 1999).

For these reasons, the three TAs (Fig. 1) were selected as model precursors of $_{aq}$SOAs due to their atmospheric abundance and tendency to reside in hydrometeors under certain conditions, but also to represent similar, cyclic TAs. R1-3 were carried out in a custom-built photochemical reactor. Product studies were conducted using gas (GC) and liquid chromatography (LC) coupled with mass spectrometry (MS). Previously reported and newly identified products were quantified with authentic and surrogate standards. Based on these data and the proposed mechanisms of R1-R3, kinetic box models were developed. These kinetic models were combined with the air-water partitioning coefficients of the reactants to estimate the yields of $_{aq}$SOA from R1-3 (Jain et al., 2024).

2 Experimental section

2.1 Materials and reagents

The reagents are listed in Section S1 of the Supporting Information (SI). LC/MS-grade water was used in all experiments.

2.2 Aqueous reaction with hydroxyl radical

The reactions were carried out in the aqueous photoreactor (Jain et al., 2024). The reaction vessel was a jacketed borosilicate glass reaction flask with an internal volume of 0.1 L and irradiated with four UVB lamps (Philips, PL-S 9W/01/2P 1CT, λ_{max} = 310 nm). The lamps were mounted inside a circular chamber (ID 10 cm, height 18 cm) and air-cooled with a fan underneath the reaction vessel. The reactor was placed on a small pedestal with a built-in magnetic stirrer to mix the reaction mixture. The reaction mixture was maintained at 298K using a circulating water bath (SC100 a10, Thermo Fisher Scientific) connected to the outer jacket of the reaction flask.

2.3 Experimental procedures

Hydrogen peroxide (H_2O_2) was a photolytic precursor of OH. The aqueous reaction solution (0.1 ml) contained a mixture of one of MTA (0.6 mM) and H_2O_2 (0.09 M). After the reactants were dissolved, the solution was filtered through a 0.7-µm GF syringe filter. Before initiating the reaction, the lamps were warmed up for 30 min, and the solution temperature was stabilized at 298 K. The reaction was carried out for 30-35 min, and up to 16 aliquots of the reaction mixture were sampled. For LC/MS analyses, each aliquot was filtered through a 0.22 µm syringe filter (PTFE) and injected. For GC/MS analyses, 800 µl of the reaction solution was saturated with sodium chloride and extracted with 300 µl of ethyl acetate containing 0.6 mM dimethyl phthalate, used as an internal standard for peak area normalization. Afterward, the organic layer was dried with anhydrous sodium sulphate and injected into the GC/MS instrument.

https://doi.org/10.5194/egusphere-2026-1788
Preprint. Discussion started: 18 May 2026

2.4 Product studies

Precursors and products were quantified with GC-EI/MS and identified with GC-NCI/MS and LC-ESI/MS.

The molar yields of the products were calculated with Eq. (1).

$$[Product]_t = Yield \times \Delta[MTA]_t \quad (1)$$

In Eq. (1), $[Product]_t$ is the concentration of a product at time t, from the onset of the reaction (in mM). $\Delta[MTA]$ is the amount of the MTA consumed at time t (mM). The yields were derived as slopes of the linear portion of the plots obtained with Eq. (1) (Gierczak et al., 2021).

Products were quantified with authentic standards whenever possible. At the same time, the vast majority of analytes were quantified with surrogate standards – Section S3. For some products, due to the lack of appropriate surrogate standards and other analytical problems (e.g., very low signal intensity), the yields were derived by fitting the kinetic model (section 2.5) to the experimental data.

2.5 Kinetic models

Kinetic modeling was performed with the Java version of Acuchem (Braun et al., 1988). Based on the measured product yields and the proposed mechanism, R1-R3 kinetic box models were developed – Section S2. The models describe the formation of the detected first and second-generation products of R1-R3 (Tables S2-S4). Most $k_{OH_{aq}}$ values used in the models (Tables S2-S4) were predicted with SAR (Witkowski et al., 2024b). The unknown product yields in models were adjusted by fitting the temporal concentration profiles of the reactants to the experimental data.

2.6 Yields of aqueous secondary aerosols

Yields of $_{aq}$SOAs from R1-R3 were derived assuming that all reactants, at any given time, partition between aqueous and gas phases according to the Henry's Law equilibrium – Eq. (2).

$$SOA_{aq}yield(\%, w/w) = \frac{\sum \%_{aq} \times c_{reactant}(t)}{\Delta MTA(t)} \quad (2)$$

In Eq. (2), $_{aq}$SOAs yield (%, w/w) is the mass yield of organic aerosols, $\Delta MTA(t)$ is the amount (g×L^{-1}) of the precursor consumed at time t, $\%_{aq}$ is the mass fraction of reactant in the aqueous phase, which is multiplied by the concentration of this reactant (g×L^{-1}). The fraction of each reactant in the aqueous phase was derived with Eq. (3).

$$\%_{aq}(LWC) = 1 - \frac{1}{1 + H^{cc} \times volumeofwater(m^3)} \quad (3)$$

In Eq. (3), $\%_{aq}$ is the fraction for each reactant in the aqueous phase, which depends on LWC, and is obtained using the dimensionless Henry law constants (H^{cc}) in Eq. (3) is multiplied by the volume of water in 1 m^3 of air. Experimentally measured values were used whenever available, but the majority of H^{cc} values used in the models were predicted with HenryWin v4.11 – Tables S5 – S7 (Episuite4.11).

https://doi.org/10.5194/egusphere-2026-1788
Preprint. Discussion started: 18 May 2026

2.7 Chromatographic analyses

Qualitative and quantitative analyses were carried out using GC/MS equipped with electron ionization (EI) and negative chemical ionization (NCI) ion sources, and LC/MS equipped with an electrospray ionization (ESI) ion source.

2.7.1 Gas chromatography coupled with mass spectrometry

GC/MS analyses were performed using a GC/MS-2010 Ultra gas chromatograph coupled with a single quadrupole mass spectrometer (Shimadzu) equipped with electron ionization (EI) or negative chemical ionization (NCI) ion source.
Precursors and products of R1-3 were separated with a VF-WAXms column: 30 m × 0.25 mm × 0.5 µm and quantified in the EI mode. The column flow was 0.67 ml/min, and the purge flow was 2 ml/min; the split ratio was set to 20. The injector, ion source, and mass spectrometer transfer line temperatures were set at 250°C. The temperature program involved an initial hold at 70 °C for 4 min, followed by a linear increase at a rate of 15 °C/min to 250°C, a 6 min hold. The MS was operating in scan (m/z = 50-300) and SIM modes (Table S9-S11).
Quantitative analyses were carried out in the NCI mode using methane and ammonia as reagent gases. In these analyses, a ZB-5MSplus column (30m×0.25 mm×0.25 µm) was used. The column flow was 0.68 ml/min, and the purge flow was 2 ml/min; the injection volume was 0.5 µl in splitless mode. The temperatures of the injector, ion source, and mass spectrometer transfer line were 280°C. The temperature program included an initial hold at 50 °C for 2 min, followed by a linear increase at a rate of 16 °C/min to 70°C, for 8 min hold, another linear increase at a rate of 10°C/min to 170°C, a 5 min hold, then a linear increase at a rate of 15 °C/min to 250°C, with a 1 min hold. The MS operated in the scan mode (m/z = 50-300).

2.7.2 Liquid chromatography coupled with time-of-flight mass spectrometry

Analyses were carried out with a Waters ACQUITY UHPLC liquid chromatograph coupled with the Xevo G2 ToF/MS equipped with an ESI source operating in the negative ionization mode. The ESI source conditions were: source temperature 100°C, offset 80V, desolvation temperature 350°C, capillary voltage: 2.8kV, sampling cone: 40V, cone gas: 50L/h, desolvation gas 700L/h. The analytes were separated using a BEH C18 column (Waters), 100 × 2.1 mm ×1.7 µm. Eluent A was 0.2% formic acid solution in water (pH ≈ 2.8), and eluent B was ACN with 0.2% formic acid. The flow rate of the mobile phase was 0.25 ml/min, and the column temperature was maintained at 40°C. A gradient elution program was used: initially 5%B for 5 min, then linear increase to 45%B over 15 min, then linear increase to 95% B over 2 min, kept for 2 min, then decrease to 5% B over 1 min, kept for 2 min. Total runtime was 27 min.

2.8 Control experiments and uncertainty

Control measurements performed without adding H_2O_2 to the reaction solution confirmed that the MTAs under investigation (Fig. 1) were not photolyzed with the UVB radiation used to generate OH (section 2.2). Also, no “dark” reactions (within the

https://doi.org/10.5194/egusphere-2026-1788
Preprint. Discussion started: 18 May 2026

timescale of the experiments) were observed between the precursors and H_2O_2 while the reactor lamps were kept off. All measurements were carried out at least three times.

3 Results and discussion

3.1 Mechanism of OH reaction with fenchol

The neutral products of R1 were detected with GC/MS – Fig. 2.

https://doi.org/10.5194/egusphere-2026-1788
Preprint. Discussion started: 18 May 2026

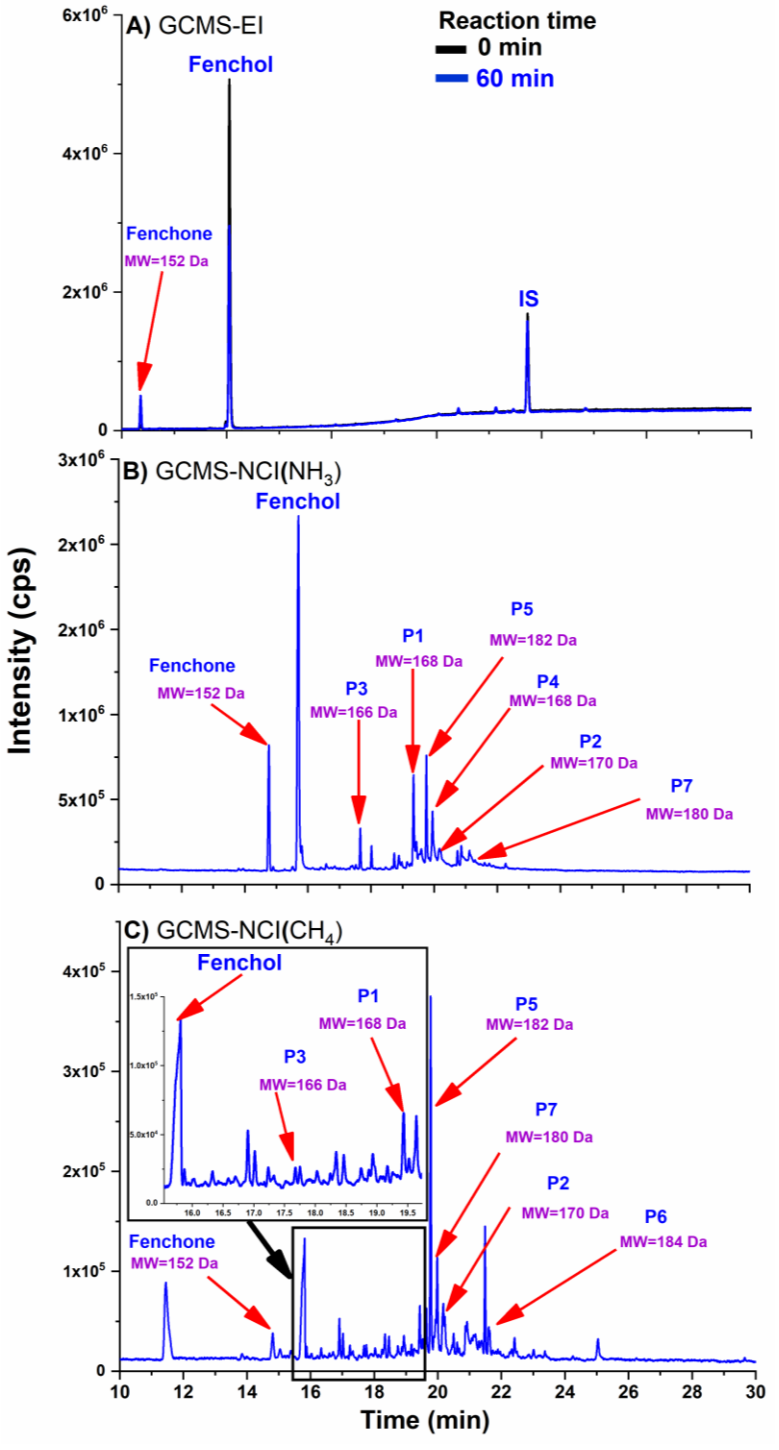

205

Figure 2: GC/MS chromatograms of the products of fenchol (FCH) + OH reaction (R1) detected with EI (A) and, NCI using NH_3 (B), and CH_4 (C) as reagent gases. Note that different chromatographic columns were used for GC-EI/MS and GC-NCI/MS analyses (section 2.7.1), resulting in different retention times.

https://doi.org/10.5194/egusphere-2026-1788
Preprint. Discussion started: 18 May 2026

In the EI mode, only the formation of fenchone from R1 was observed (Fig. 2A). Additional products were detected with NCI, due to the higher sensitivity for products P1-P7 in the NCI mode (Fig. 2B and C) (Javelle et al., 2021). Similar results were obtained for both reagent gases, but the sensitivity was significantly higher for NH_3. For this reason, neutral products of R1-R3 were identified based on the data obtained for NH_3.

Moreover, the results of LC-ToF/MS analyses confirmed the formation of TACs from R1- Fig. 3.

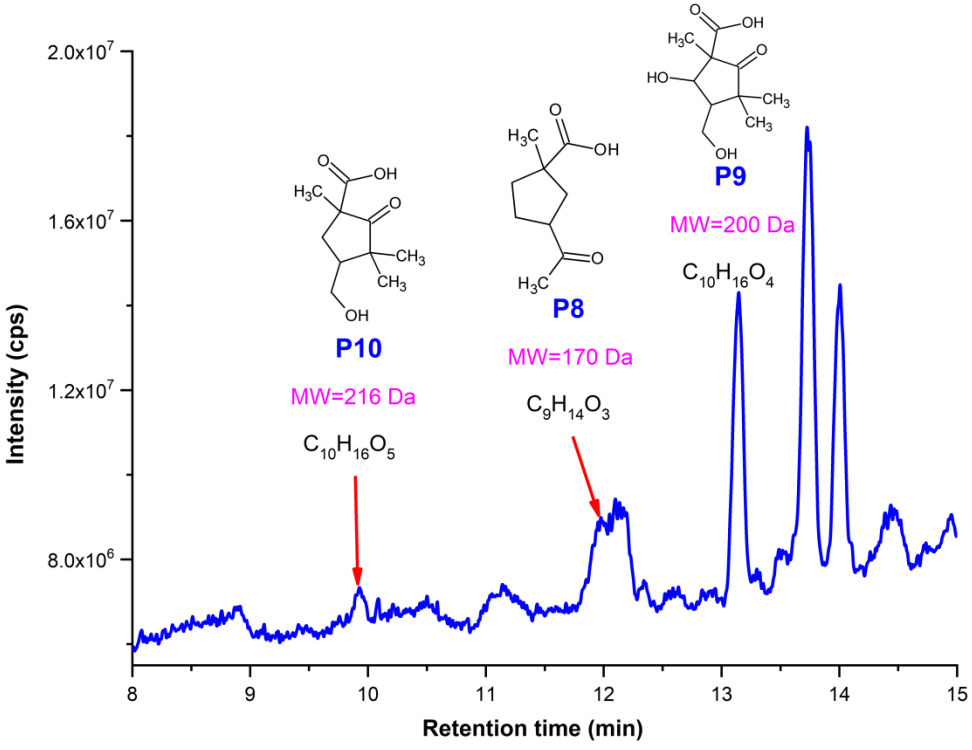

Figure 3: LC-ToF/MS chromatogram of TACs formed from OH reaction with fenchol – R1.

Elemental compositions of TACs (P8-P10) formed from R1 were derived with LC-ToF/MS - Table S12. The mechanism proposed for R1 is based on the structures of the neutral (Fig. 2) and acidic (Fig. 3) products and their formation yields (Tables S8 and S9). The yields of the products (Table S7) indicated that the major products of R1 were fenchone, P2, and P4-P6, with pathways I and II (Scheme 1) accounting for 85% and 12% of the total yields of the products, respectively. Pathways III and IV in Scheme 2, were minor channels, contributing about 3% to the total yield of R1 products – Table S8.

https://doi.org/10.5194/egusphere-2026-1788
Preprint. Discussion started: 18 May 2026

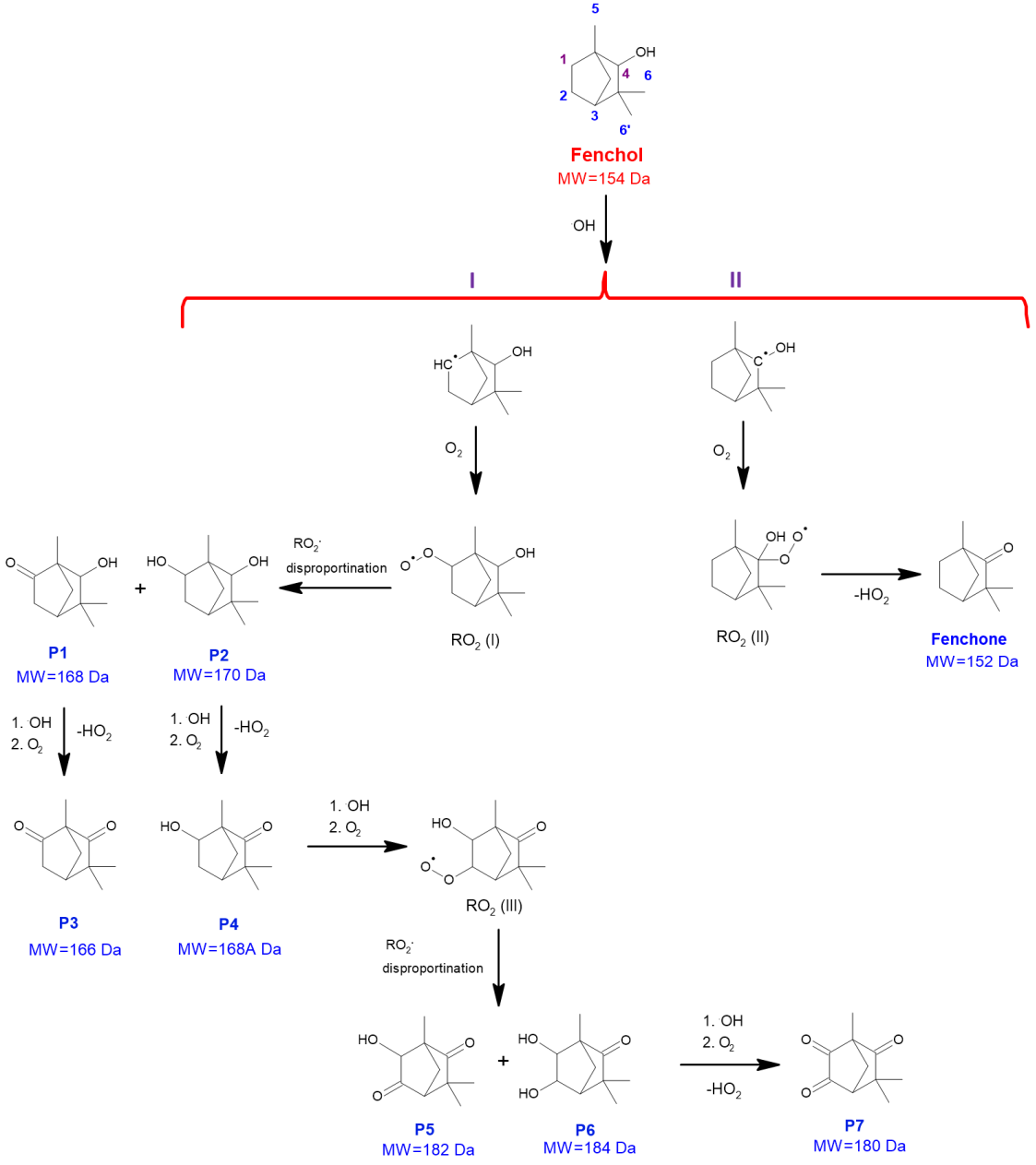

Scheme 1: Proposed mechanism of fenchol + OH reaction (R1). The products detected in this work are highlighted in blue bold font. The formation of all possible isomers is not included for clarity. The mechanism of R1 is continued in Scheme 2 – oxidation of fenchone.

In Scheme 1, pathway (I) yields peroxy radical RO_2(I), which undergoes the Russell disproportionation reaction to produce carbonyl (P1) and alcohol (P2) products (Fig. 2) (Russell, 1957). Products P1 and P2 can further be converted to P3 and P4 following the conversion of -OH to a carbonyl moiety, analogous to pathway II (Scheme 1). P3 exhibits lower predicted

https://doi.org/10.5194/egusphere-2026-1788
Preprint. Discussion started: 18 May 2026

($k_{OH_{aq}}$=1.9×10^9 M^{-1}s^{-1}) than P4 ($k_{OH_{aq}}$=2.7×10^9 M^{-1}s^{-1}) (Witkowski et al., 2024a). Consequently, P4 is oxidized faster than P3, yielding RO_2(III), which then produces a carbonyl (P5) and an alcohol (P6) (Russell, 1957). Likewise, P6 ($k_{OH_{aq}}$=2.8×10^9 M^{-1}s^{-1}) is oxidized preferentially over P5 ($k_{OH_{aq}}$=1.8×10^9 M^{-1}s^{-1}), resulting in P7 – Scheme 1 (Witkowski et al., 2024a). In pathway II, FCH is converted to fenchone by elimination of HO_2 following the H-atom abstraction from the α-position of -OH (Denisov and Khudyakov, 1987; Puchkov et al., 2005; Puchkov et al., 2013; Bradley et al., 2001).

Considering the well-known reactions of RO and RO_2 radicals, proposing a feasible mechanism for the formation of TACs (Fig. 3) directly from FCH is difficult. Consequently, in the proposed mechanism (Scheme 2), P8-P10 are second-generation products of R1 formed from fenchone.

https://doi.org/10.5194/egusphere-2026-1788
Preprint. Discussion started: 18 May 2026

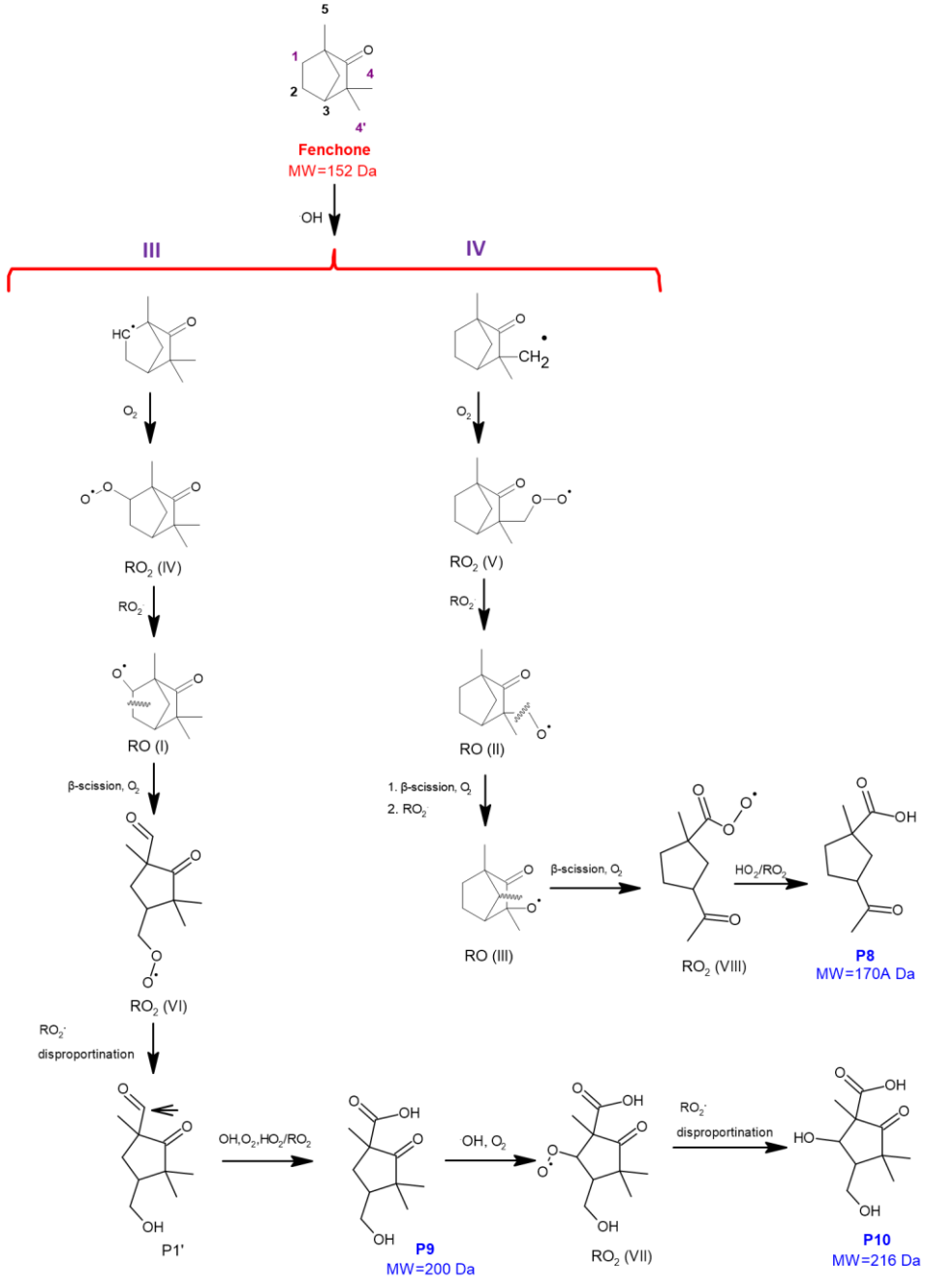

Scheme 2: Proposed mechanism for the OH reaction with fenchone. The products detected with LC-ToF/MS are highlighted in blue bold font.

In Scheme 2, RO_2(IV) and RO_2(V) are formed by the H-atom abstraction from the C1 and C4/4′ positions of fenchone, respectively. Pathway III in Scheme 2 involves the formation of RO_2(IV), which then undergoes a β-scission reaction, resulting in RO_2(VI). RO_2(VI) yields by-product P1˙, which is then likely rapidly oxidized to P9 following OH attack on the

https://doi.org/10.5194/egusphere-2026-1788
Preprint. Discussion started: 18 May 2026

aldehyde moiety (Scheme 2) (Enami and Sakamoto, 2016a). Subsequently, P9 can undergo further oxidation to P10 via the addition of the -OH moiety to the cyclopentane ring. Pathway (IV) yields RO_2(V), which forms P8, following two consecutive β-scission reactions (Enami and Sakamoto, 2016a).

Previously, only the formation of fenchone and products P5-P7 from R1 in the gas phase was confirmed with GC/MS (Ceacero-Vega et al., 2012). At the same time, the formation of TACs from R1 was not reported, likely because low quantities of underivatized TACs are difficult to detect with GC/MS (Ceacero-Vega et al., 2012). Hence, this work is the first to report the formation of low-volatility TACs from R1.

3.2 Mechanism of OH reaction with borneol

The mechanism of R2 (Schemes 3 - 5) was proposed based on the products identified with GC/MS (Fig. S2), LC-ToF/MS (Fig. S3), and their formation yields (Table S7 and S8). The major products of R2 were camphor, products P1-P3, and P6-P8, accounting for 88% of the molar yield of the products (Tables S8 and S9). Minor pathways IV (2%, Scheme 4) and V and VI (3%, Scheme 5) accounted for ca. 5% of the total yield.

https://doi.org/10.5194/egusphere-2026-1788
Preprint. Discussion started: 18 May 2026

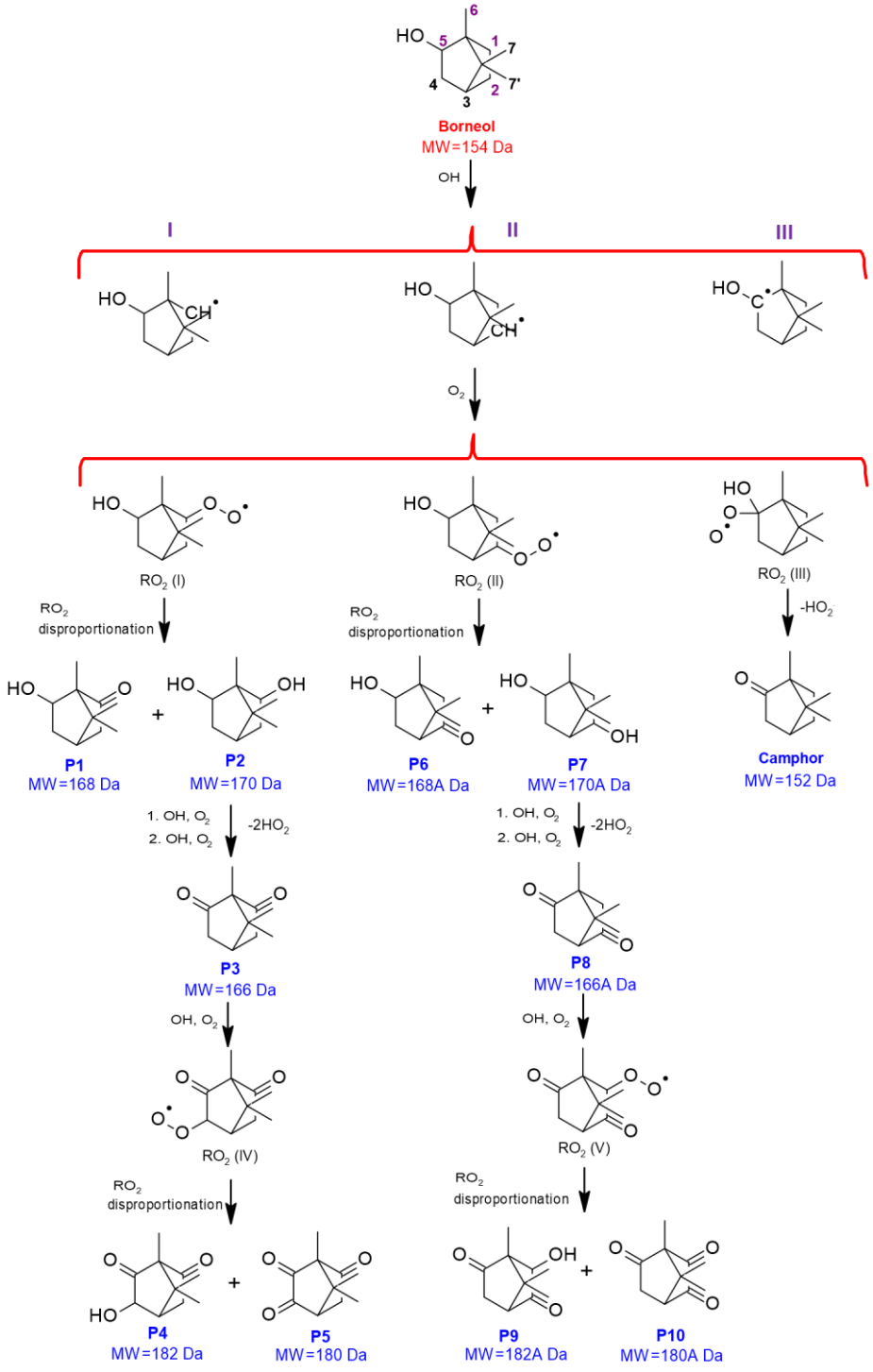

https://doi.org/10.5194/egusphere-2026-1788
Preprint. Discussion started: 18 May 2026

Scheme 3: Proposed mechanism of borneol (BNL) + OH reaction (R2). The detected products are highlighted in blue bold font. The formation of all possible isomers is not included for clarity. The mechanism of R2 is continued in Schemes 4 and 5 – formation of TACs.

In Scheme 3, RO_2(I) and RO_2(II) are formed via pathways I and II, respectively. Formation of P1-P2 and P6-P7 can be explained via disproportionation reactions of RO_2(I) and RO_2(II) (Russell, 1957). Diols: P2 ($k_{OH_{aq}}$=3.4×10^9 M^{-1}s^{-1}), P7 ($k_{OH_{aq}}$=3.3×10^9 M^{-1}s^{-1}) are likely oxidized faster than P1 ($k_{OH_{aq}}$=2.6×10^9 M^{-1}s^{-1}) and, P6 ($k_{OH_{aq}}$=2.4×10^9 M^{-1}s^{-1}), (Witkowski et al., 2024a). For this reason, dicarbonyls P3 and P8 are formed by the H-atom abstraction from the α-position of -OH moieties in P2 and P7, followed by the elimination of – HO_2. The conversion of BNL to camphor (pathway III in Scheme 3) likely occurs via the same mechanism (Denisov and Khudyakov, 1987; Puchkov et al., 2005; Puchkov et al., 2013; Bradley et al., 2001). In Scheme 3, P3 and P8 can undergo further oxidation, resulting in P5, P10, and P4, P9. The formation of products P1, P2, P6, and P7 from R2 was also observed in the gas phase, likely occurring via similar pathways (Ceacero-Vega et al., 2012).

The formation of TACs (detected with LC/MS - Fig. S3) from camphor was again more feasible, but the acidic product P12 may be produced directly from the precursor, involving the H-atom abstraction from the C6 position of BNL – Scheme 4.

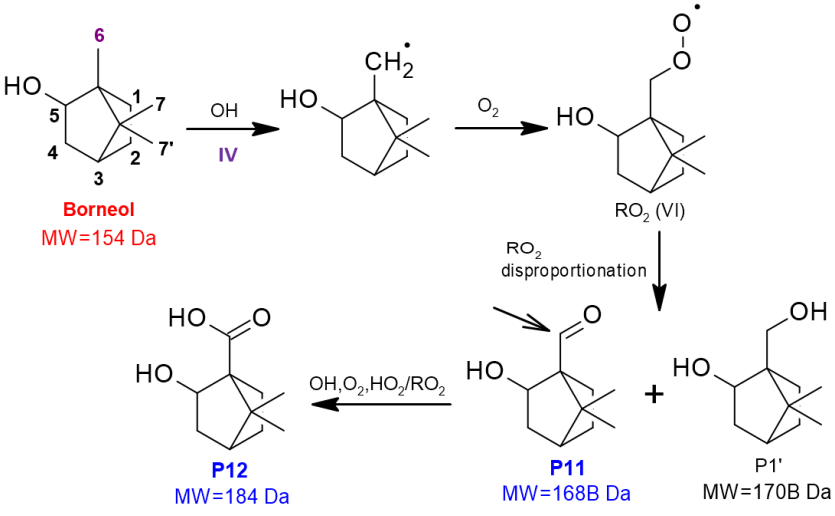

Scheme 4: Formation of P12 from OH reaction with borneol (R2) via pathway IV, involving the H-atom abstraction from the C6.

In Scheme 4, pathway (IV) yields RO_2(VI), which undergoes the disproportionation reaction, resulting in P1′ and P11. P11 is further oxidized to P12 (Enami and Sakamoto, 2016b). The two by-products formed by pathway (IV) – P11 and P1' - were not detected, likely due to their low formation yields and rapid conversion of P11 to P12. Camphoric acid and P14 formed from R2 were most likely produced from camphor – Scheme 5.

https://doi.org/10.5194/egusphere-2026-1788
Preprint. Discussion started: 18 May 2026

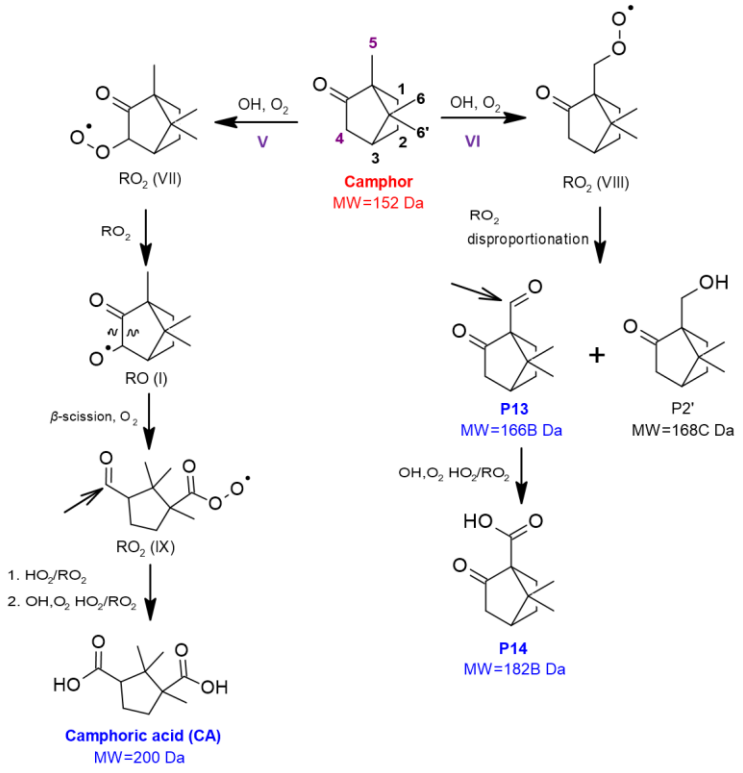

Scheme 5: Proposed mechanism for OH reaction with camphor. The products detected (camphoric acid and P14) are highlighted in blue bold font.

Camphoric acid is formed via pathway V (Scheme 5), which is analogous to pathway III in Scheme 2, and P14 is produced via pathway (VI), analogously to pathway IV in Scheme 4 (Enami and Sakamoto, 2016b).

3.3 Mechanism of OH reaction with menthol

The mechanism of R3 (Schemes 6 and 7) was proposed based on the products identified with GC/MS (Fig. S4), LC-ToF/MS (Fig. S5), and their formation yields (Tables S8 and S9). The major channels of R3 were pathways I (54%) and II (42%) (Scheme 6). The yield of menthone formed from R3 (pathway III) was approx. 3%, the lowest of the two MTAs under investigation. Minor channels of R3 were pathways IV- VI (Scheme 7), with contributed approx. 1% of the total yield of the products.

https://doi.org/10.5194/egusphere-2026-1788
Preprint. Discussion started: 18 May 2026

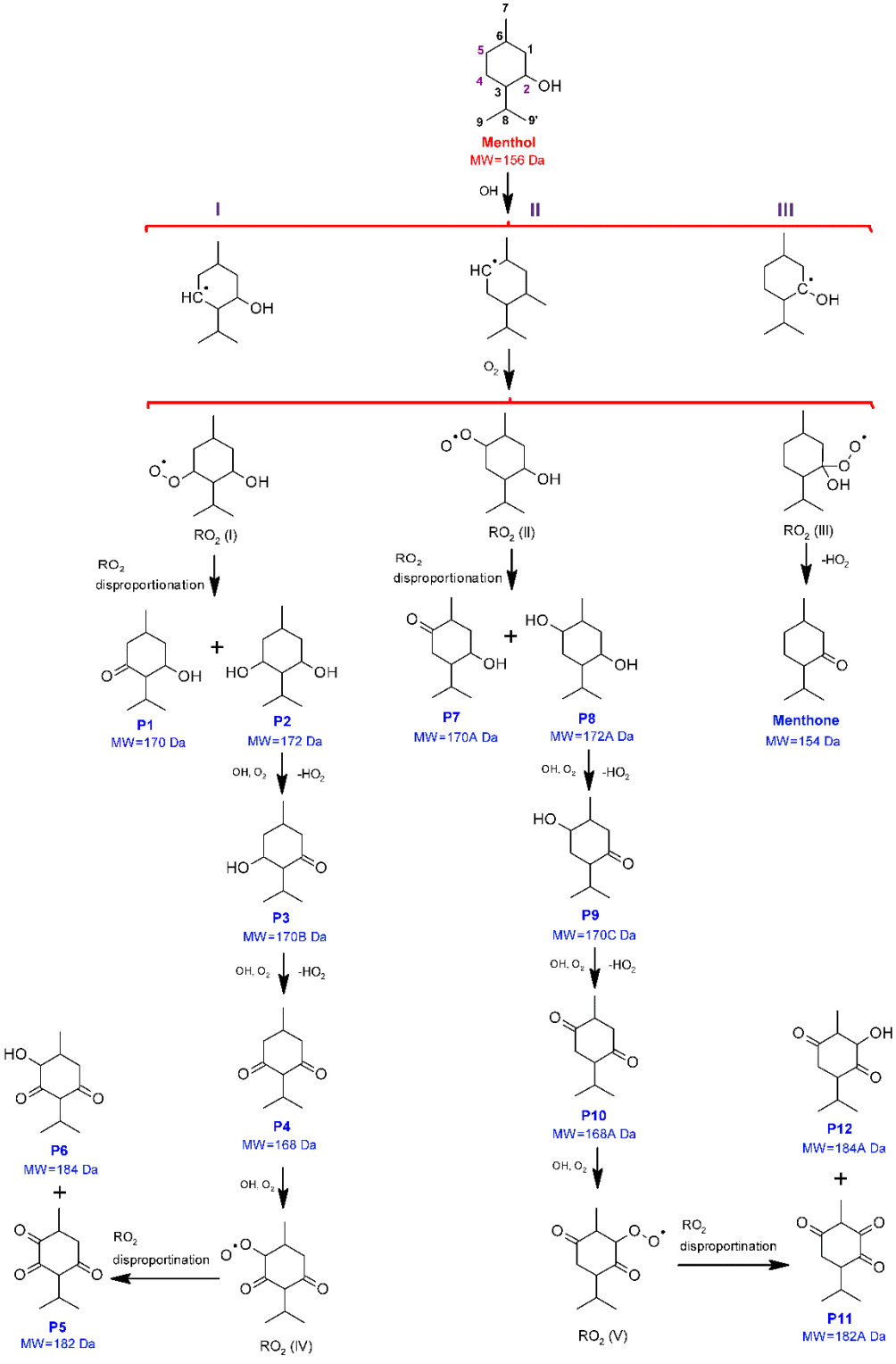

290

https://doi.org/10.5194/egusphere-2026-1788
Preprint. Discussion started: 18 May 2026

Scheme 6: Proposed mechanism of menthol (MTH) + OH reaction (R3). Products observed in this work are highlighted in blue bold font. The formation of all possible isomers is not included for clarity. The mechanism of R3 is continued in Scheme 7 – oxidation of menthone.

In Scheme 6, RO_2(I) and RO_2(II) are formed via pathways I and II, respectively, and undergo the disproportionation reaction, leading to pairs of isomeric products: P1, P7, and P2, P8. Afterward, products P3 and P9 are formed by oxidation of P2 ($k_{OH_{aq}}$=6.1×10^9 M^{-1}s^{-1}), and P8, ($k_{OH_{aq}}$=5.7×10^9 M^{-1}s^{-1}), which likely react faster than P1 ($k_{OH_{aq}}$=4.3×10^9 M^{-1}s^{-1}) and P7 ($k_{OH_{aq}}$=4.1×10^9 M^{-1}s^{-1}), respectively – Scheme 6 (Witkowski et al., 2024a). In pathways I and II, the elimination of HO_2 from P3 and P9 results in P4 and P10, respectively. Further oxidation of P4 and P10 results in P5, P6, and P11, P12, which are formed by the disproportionation mechanism (Scheme 6). The formation of menthone from R3 (pathway III is Scheme 6) is analogous to the formation of fenchone and camphor from R1 and R2, respectively. TACs formed from R3 (Fig. S5) are likely second-generation products, produced by the oxidation of menthone – Scheme 7.

https://doi.org/10.5194/egusphere-2026-1788
Preprint. Discussion started: 18 May 2026

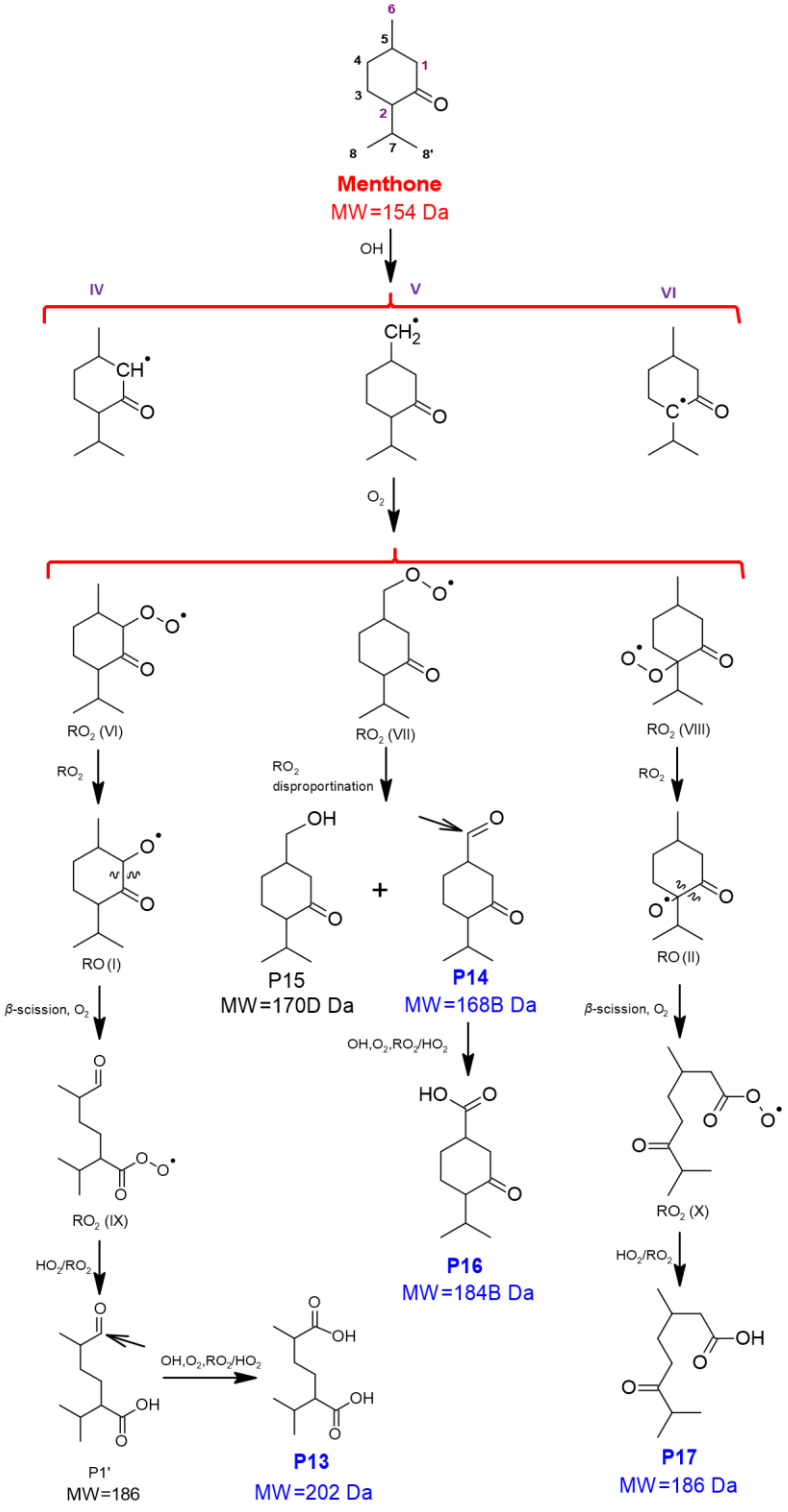

https://doi.org/10.5194/egusphere-2026-1788
Preprint. Discussion started: 18 May 2026

Scheme 7: Proposed mechanism of the OH + menthone reaction. Products observed in this work are highlighted in blue.

The mechanisms of P13, P16, and P17 formation from R3 in Scheme 7 are analogous to the formation of TACs from R1 and R2. Pathway (IV-VI) in Scheme 7 yields corresponding RO_2 radicals. Afterward, RO_2(IV–VI) are converted to P13, P16, and P17 via the β-scission and disproportionation reactions (Enami and Sakamoto, 2016b). The formation of carboxylic moieties in P13, P14, P16, and P17 involves an H-atom from the α-positions of the corresponding aldehyde by-products (Enami and Sakamoto, 2016b).

3.4 Mechanism of OH reaction with fenchol, borneol, and menthol

Over 88% of the R1-R3 products were quantified using the experimental approach used in this work- Fig. S1. For all precursors under investigation, the major products were neutral molecules containing -OH and C=O moieties, and the yields of TACs were between 1 and 5% – Table. 1.

Table 1. The yield of neutral and acidic products of the aqueous OH reaction with fenchol (R1), borneol (R2), and menthol (R3) obtained in this work.

Precursor	**Molar yields**		
	Neutrals[a]	Acids[b]	Total[c]
Fenchol	0.91±0.07	0.03	0.94±0.07
Borneol	0.95±0.10	0.05	0.99±0.10
Menthol	0.87±0.05	0.01	0.88±0.05

[a]Measured with authentic or surrogate standards [b]Values obtained from the kinetic models [c]Uncertainties derived from the experimental uncertainties of the yields of individual

The measured yields of some products were very high: 40-54% - Table S7. At the same time, the partial aqueous SAR (Fig S6) indicated that none of the aliphatic H-atoms in FCH, BNL, and MTH were so strongly favored (Witkowski et al., 2024b). SAR also indicated high rates of H-atom abstraction from the CH_3 groups. However, H-atom abstraction from the cyclohexane ring better explains the formation of the major (non-acidic) products of R1-R3.

The apparent discrepancies between SAR predictions and experimental data can be due to the formation of isomeric products, which are not completely resolved by GC/MS (see Figs. 1, S2, and S4). As denoted in Schemes 1, 3, and 6, it is reasonable to assume that isomeric products can be formed by adding the -OH and C=O moieties to the original carbon skeleton at different positions, resulting in a relatively large number of possible isomers. Also, except for the first-generation ketones (fenchone, camphor, and menthone), the rest of the products were quantified with surrogate standards (Tables S10-S12), which may result in higher uncertainties in their yields.

The reactions of OH with MTH, FCH, BNL, and cyclohexanol were previously investigated in the gas phase. The yields of the corresponding ketones from the OH reaction with FCH, BNL, and cyclohexanol in the gas phase are significantly higher than in the aqueous phase – Table 2.

https://doi.org/10.5194/egusphere-2026-1788
Preprint. Discussion started: 18 May 2026

Table 2. Yields of corresponding ketones formed from the OH reaction with fenchol, borneol, menthol, and cyclohexanol in the gas and aqueous phases.

		Yield (%)		Reference
Alcohol (recursor)	Ketone (product)	*Aqueous phase*[a]	*Gas-phase*	
Fenchol	Fenchone	0.11±0.01	0.61±2.6	(Ceacero-Vega et al., 2012)
Borneol	Camphor	0.12±0.02	0.49±1.0	(Ceacero-Vega et al., 2012)
Menthol	Menthone	0.03±0.00	-	
Cyclohexanol	Cylcohexanone	-	0.55±0.6	(Bradley et al., 2001)

[a]Measured with authentic standards

In the gas phase, the measured yields of ketones from the reaction with OH with the cyclic alcohols were between 0.49 and 0.61 - Table 2(Ceacero-Vega et al., 2012; Bradley et al., 2001). These data indicate that H-atom abstraction from the -OH moiety α-position was the main reaction pathway. This conclusion is also supported by the partial $k_{OH_{aq}}$ values estimated with the gas-phase SAR (Kwok and Atkinson, 1995; Ceacero-Vega et al., 2012).

At the same time, the aqueous SAR predicts that the abstraction of the H-atom adjacent to the -OH group contributes 5-15% to the total $k_{OH_{aq}}$ – Fig. S6. The values of partial rate coefficients predicted with the aqueous SAR (Fig. S6) are within the range of the measured yields of primary carbonyls, ranging from 3 to 12 % - Table 2 (Witkowski et al., 2024b).

This different intramolecular selectivity for the H-atom abstraction by OH from cyclic alcohols in gas and aqueous phases may be attributed to solvent effects, including the water cage effects (Kopinke and Georgi, 2017), H-bond formation (Otto and Engberts, 2003). In water, the reaction of OH with aliphatic, oxygenated molecules likely involves the formation of a highly polarized transition state (TS), which is stabilized by the solvent (Mitroka et al., 2010). At the same time, -OH groups can compete for the electron density with the attacking OH, which lowers the TS stabilization. This phenomenon is reflected by the values of the empirical F (α-position) substituent factor for -OH moiety in the gas (3.5) and aqueous (1.9) SARs, showing the lower net activating effect in water (Kwok and Atkinson, 1995; Witkowski et al., 2024b).

3.5 Kinetic models

The kinetic models for R1–R3 are based on the measured product yields (Tables S8 and S9) and their proposed formation pathways (Schemes 1-7). For all precursors, good agreement between the experimental data was obtained; sample results obtained for R1 are presented in Fig. 4.

https://doi.org/10.5194/egusphere-2026-1788
Preprint. Discussion started: 18 May 2026

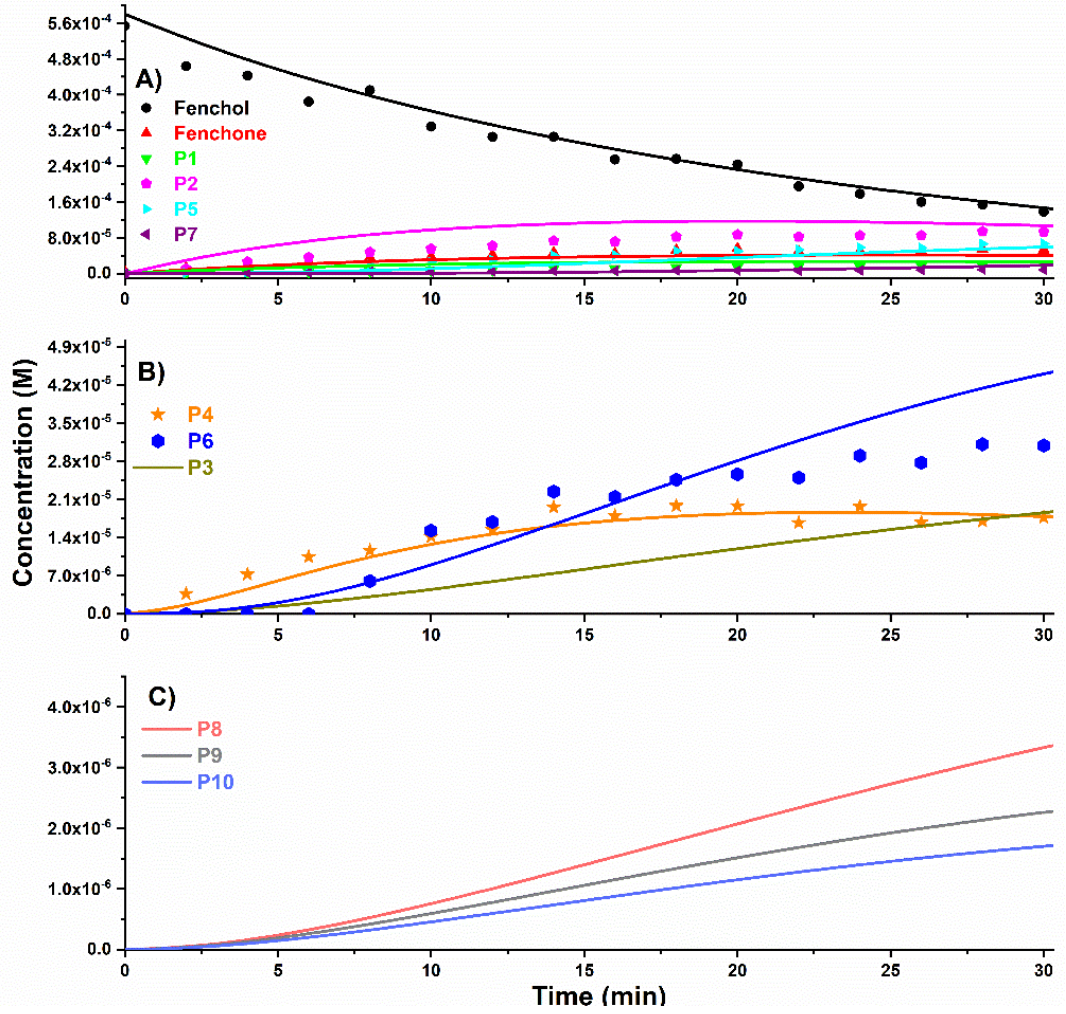

Figure 4: Measured and modeled temporal evolution of the reactants for fenchol + OH reaction (R1). Points represent experimental data, and lines are the temporal profiles generated by the model. Structures of neutral (A and B) and acidic (C) products are shown in Schemes 1 and 2, respectively.

For R1, the box model accurately predicted the temporal evolution of the reactants - Fig. 4A, B. Only model data is shown for TACs and some neutral products since their yields were not measured - (section 3.4). Very similar, satisfactory performance of the models was obtained for R2 and R3 - Figs. S7 and S8.

4 Atmospheric implications

As discussed in our previous work, R1-R3 can be relevant in the atmosphere for LWC≥ 0.1 g × m^3 (Witkowski et al., 2024a). The $k_{OH_{aq}}$ values measured in our previous study indicated that liquid water affects the lifetimes of MTH, FCH, and BNL in clouds, fogs, and rain. The lifetimes, estimated for the average $[OH]_{aq}$ between 3.5×10^{-15} M (urban clouds) and

https://doi.org/10.5194/egusphere-2026-1788
Preprint. Discussion started: 18 May 2026

2.2×10^{-14} M (remote clouds), ranged from 10 to 300 h (Bianco et al., 2020). The lower limit estimate is comparable with the time an air parcel spends inside the cloud, which was estimated at 18 h (Herrmann et al., 2015). Furthermore, the lowest lifetimes, on the order of minutes, were obtained for marine clouds with the average $[OH]_{aq} = 2.2\times10^{-12}$ M (Witkowski et al., 2024a). Even though the three TAs under investigation have no documented emission sources from marine biota, reaction in marine clouds may still be relevant due to the (long-range) atmospheric transport and near the shoreline (Coggon et al., 2014).

Furthermore, these lifetime estimates only consider OH diffusion from the gas phase following the Henry's law equilibrium (Sarang et al., 2021). At the same time, OH can also be formed in cloud water, which involves the photolysis of H_2O_2 and organic hydroperoxides, Fenton-like reactions, and ozonolysis of dissolved organic matter (Kuang et al., 2020a; Bianco et al., 2020). Such processes can increase cloud water $[OH]_{aq}$ to µM-level (Paulson et al., 2019), thereby shortening the lifetimes of semi-volatile TAs by a few orders of magnitude.

Consequently, the mass yields of $_{aq}$SOAs (section 2.6) from R1- R3 were derived for LWC values ranging from 0.03 to 3 (g × m^{-3}) - Fig. 5.

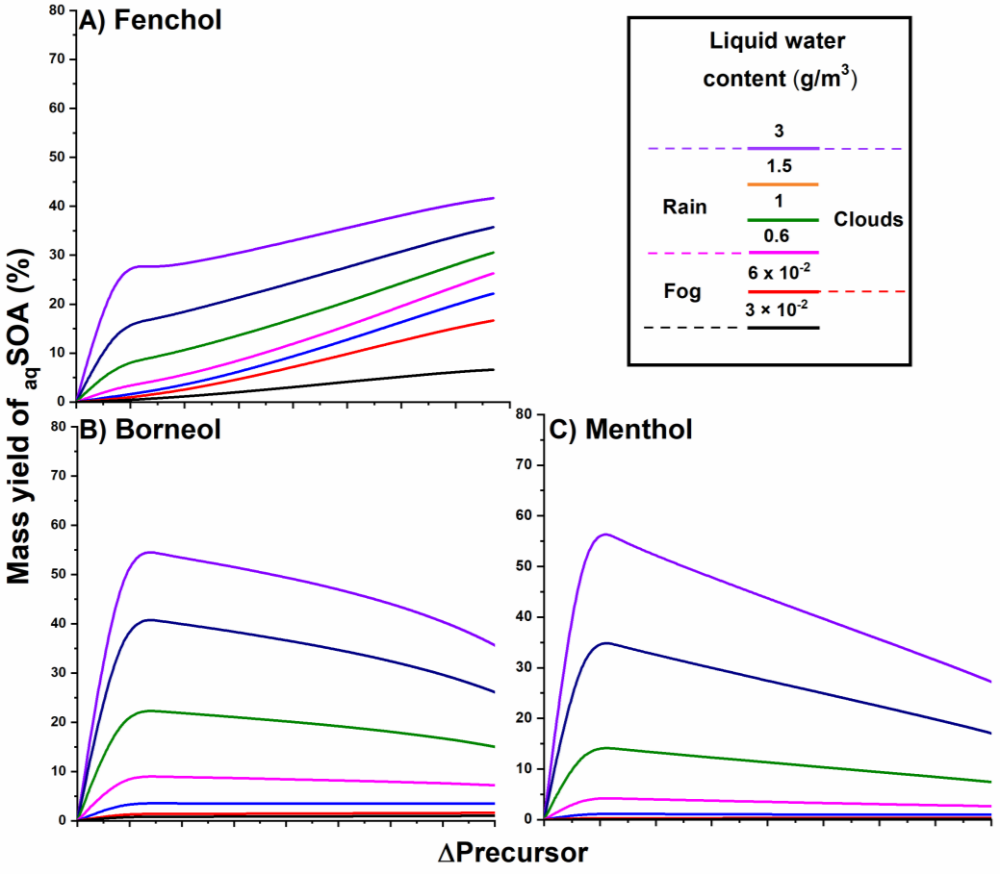

Figure 5: Modelled yields of aqSOA from fenchol (A), borneol (B), and menthol (C) as a function of LWC and reaction coordinate.

https://doi.org/10.5194/egusphere-2026-1788
Preprint. Discussion started: 18 May 2026

The main components of $_{aq}$SOA formed from R1-R3 at LWC between 0.3 – 3 (g × m^3) are the first - and second - generation TACs. However, at higher LWC, the relative contribution of neutral products, which were formed with much higher yields than TACs (Table 1), becomes dominant. The initial spikes in the mass yields of $_{aq}$SOAs are also due to the neutral products portioning into the aqueous phase – Fig. 5.

An increase in the yield of $_{aq}$SOA for FCH (Fig. 5A) at the later stages of the reaction was observed, whereas BNL and MTH exhibited the opposite trend (Figs. 5B and C). The trends observed in Fig. 5B and C are due to the loss of higher-generation (low-volatility) products during the initial and intermediate stages of the reaction (Sections 3.1 - 3.3). These higher-generation products of R2 and R3 (Table S7) are completely oxidized and thus removed by the time the precursors are consumed.

The yield of $_{aq}$SOA from R3 (Fig. 5C) was somewhat lower than that of R2 (Fig. 5B). This could be due to the absence of the bridged cyclohexane ring in MTH, resulting in a higher degree of fragmentation of the carbon skeleton, thereby lowering the yield of $_{aq}$SOAs. For instance, in a study on the atmospheric degradation of cyclohexanol by OH, greater fragmentation of the precursor was observed, resulting in the formation of straight-chain alcohols and carbonyls (Bradley et al., 2001). In contrast, precursors containing bridged cyclohexane rings yielded less fragmented oxidation products (Ceacero-Vega et al., 2012).

The increase in $_{aq}$SOA in Fig. 5A is attributed to the significantly high H^{cc} values of the products of R1, particularly P5, P7, P9, and P10 (see Schemes 1 and 2 and Table S4). Additionally, the formation of highly oxygenated TACs (P9 and P10) from R1 also contributed to the increase in the predicted $_{aq}$SOA yield in Fig. 5A. Analogous products, with very high H^{cc} values, were not formed from R2 or R3 (Table S5, S6).

The modelled yields of $_{aq}$SOA from R1-3 are between 10 and 70% (Fig. 5). In the gas phase, the yields of $_{gas}$SOA of 49.0±1.0% for BNL and 60.9±2.6% for FCH were reported (Ceacero-Vega et al., 2012). These values are comparable with the upper estimate of the $_{aq}$SOA yields obtained here (Fig. 5). Hence, the formation of gas or aqueous SOAs from R1-R3 will strongly depend on the availability of liquid water.

It is difficult to constrain the emission fluxes of individual TAs, including FCH, BNL, and MTH. The global flux of TAs from biogenic sources was estimated at 14.6 Tg yr^{-1} (Guenther et al., 2012), comparable with the emission of 34 major MTDs of 14.9 Tg yr^{-1} (Guenther et al., 2012). Hence, the emission of FCH, BNL, and MTH can be roughly estimated at 1.5 Tg×yr^{-1}, the global flux of $_{aq}$SOAs from R1- R3 can be as high as 0.15 Tg×yr^{-1}, assuming the upper yield of 70% and the availability of liquid water at 20% (Amorim et al., 2020; Hoffmann et al., 2018; Prisle, 2021). Consequently, the contribution of $_{aq}$SOAs from R1- 3 to the global flux of BSOAs is <1% (Sporre et al., 2020; Kelly et al., 2018). Further constraining the contribution of R1- 3 to the global BSOAs burden would require a more advanced atmospheric modelling, which was beyond the scope of this work.

At the same time, the local emissions of MTDs are often much higher. For instance, the emissions of MTDs from California sage plants were dominated by camphor, accounting for 57% of the emissions, with camphene and eucalyptol accounting for 7% and 13%, respectively (Mehra et al., 2020). However, care should be taken when estimating SOA formation from

https://doi.org/10.5194/egusphere-2026-1788
Preprint. Discussion started: 18 May 2026

different MTDs. Even though a very similar behaviour was observed for the TAs studies in this work, the measured yields vary greatly and appear to be structure-specific, e.g., lower values were reported for linear TAs (Lee et al., 2006).

5 Conclusions

This work provides a comprehensive mechanistic and quantitative investigation of aqueous OH reaction with three representative terpenoic monoalcohols—fenchol, borneol, and menthol. The results obtained demonstrate that these semi-volatile oxygenated terpenoids efficiently undergo aqueous oxidation, primarily yielding multifunctional, non-acidic products and smaller but atmospherically important fractions of low-volatility terpenoic acids.

The near-unity molar yields of quantified products strongly indicate that the major reaction pathways were identified, enabling the development of explicit kinetic box models that successfully reproduce experimental observations. The proposed mechanisms reveal that, in contrast to the gas phase, aqueous-phase oxidation favors pathways involving H-atom abstraction from the carbon skeleton rather than the α-position of the hydroxyl group, highlighting the importance of solvation effects and different transition-state stabilization in both phases.

A key outcome of this study is the first quantitative estimation of $_{aq}$SOA mass yields from terpenoic monoalcohols, reaching up to ~70% in air masses with high liquid water content. These yields are comparable with the previously reported $_{gas}$SOA formation for related precursors, indicating that the relative importance of aqueous versus gas-phase pathways is controlled by the availability of liquid water.

Overall, the findings demonstrate that oxygenated monoterpenes, including non-acidic terpenoids, can be efficient precursors of $_{aq}$SOA. The mechanistic insights and quantitative parameters provided here offer a foundation for improved representation of multiphase SOA formation in atmospheric models.

Data availability

Data can be obtained by contacting the corresponding author.

Author contributions

B.W. designed the study and developed the methodology. P.J. and A.B. optimized the methodology, performed the experiments, analyzed, and interpreted the raw data. B.W. and T.G. supervised the study; T.G. provided the funding and infrastructure. P.J. and B.W. wrote the original draft. All authors contributed to the manuscript writing and editing.

Competing interests

The authors declare that they have no conflicts of interest.

https://doi.org/10.5194/egusphere-2026-1788
Preprint. Discussion started: 18 May 2026

Acknowledgements

This work was carried out at the Biological and Chemical Research Centre, University of Warsaw, established within the project co-financed by the European Union from the European Regional Development Fund under the Operational Programme Innovative Economy, 2007–2013.

Financial support

This project was funded by the Polish National Science Centre: grant number 2021/43/B/ST10/00931, PI: Prof. dr hab. Tomasz Gierczak.

References

Amorim, J. V., Guo, X., Gautam, T., Fang, R., Fotang, C., Williams, F. J., and Zhao, R.: Photo-oxidation of pinic acid in the aqueous phase: a mechanistic investigation under acidic and basic pH conditions, Environ. Sci.: Atmos., 1, 276-287, 10.1039/D1EA00031D, 2021.

Amorim, J. V., Wu, S., Klimchuk, K., Lau, C., Williams, F. J., Huang, Y., and Zhao, R.: pH Dependence of the OH Reactivity of Organic Acids in the Aqueous Phase, Environ. Sci. Technol., 54, 12484-12492, 2020.

Bianco, A., Passananti, M., Brigante, M., and Mailhot, G.: Photochemistry of the Cloud Aqueous Phase: A Review, Molecules, 25, 423, 2020.

Bradley, W. R., Wyatt, S. E., Wells, J. R., Henley, M. V., and Graziano, G. M.: The Hydroxyl Radical Reaction Rate Constant and Products of Cyclohexanol, Int. J. Chem. Kinet., 33, 108-117, 10.1002/1097-4601, 2001.

Braun, W., Herron, J. T., and Kahaner, D. K.: Acuchem: A computer program for modeling complex chemical reaction systems, Int. J. Chem. Kinet., 20, 51-62, https://doi.org/10.1002/kin.550200107, 1988.

Caputi, L. and Aprea, E.: Use of terpenoids as natural flavouring compounds in food industry, Recent Adv Food Nutr Agric., 3, 9-16, 2011.

Carlton, A. G., Christiansen, A. E., Flesch, M. M., Hennigan, C. J., and Sareen, N.: Multiphase Atmospheric Chemistry in Liquid Water: Impacts and Controllability of Organic Aerosol, Acc. Chem. Res., 53, 1715-1723, https://doi.org/10.1021/acs.accounts.0c00301, 2020.

Ceacero-Vega, A. A., Ballesteros, B., Bejan, I., Barnes, I., Jiménez, E., and Albaladejo, J.: Kinetics and mechanisms of the tropospheric reactions of menthol, borneol, fenchol, camphor, and fenchone with hydroxyl radicals (OH) and chlorine atoms (Cl), J. Phys. Chem. A., 116, 4097-4107, 10.1021/JP212076G/ASSET/IMAGES/JP-2011-12076G_M006.GIF, 2012.

Chaturvedi, S., Kumar, A., Singh, V., Chakraborty, B., Kumar, R., and Min, L.: Recent Advancement in Organic Aerosol Understanding: a Review of Their Sources, Formation, and Health Impacts, Water, Air, Soil Pollut., 234, 750, 10.1007/s11270-023-06772-0, 2023.

Coggon, M. M., Sorooshian, A., Wang, Z., Craven, J. S., Metcalf, A. R., Lin, J. J., Nenes, A., Jonsson, H. H., Flagan, R. C., and Seinfeld, J. H.: Observations of continental biogenic impacts on marine aerosol and clouds off the coast of California, J. Geophys. Res. Atmos., 119, 6724-6748, https://doi.org/10.1002/2013JD021228, 2014.

Decesari, S., Sowlat, M. H., Hasheminassab, S., Sandrini, S., Gilardoni, S., Facchini, M. C., Fuzzi, S., and Sioutas, C.: Enhanced toxicity of aerosol in fog conditions in the Po Valley, Italy, Atmos. Chem. Phys., 17, 7721-7731, 10.5194/acp-17-7721-2017, 2017.

Denisov, E. T. and Khudyakov, I.: Mechanisms of action and reactivities of the free radicals of inhibitors, Chemical Reviews, 87, 1313-1357, 1987.

https://doi.org/10.5194/egusphere-2026-1788
Preprint. Discussion started: 18 May 2026

Enami, S. and Sakamoto, Y.: OH-Radical Oxidation of Surface-Active cis-Pinonic Acid at the Air-Water Interface, J. Phys. Chem. A., 120, 3578-3587, 10.1021/ACS.JPCA.6B01261/ASSET/IMAGES/LARGE/JP-2016-01261G_0006.JPEG, 2016a.
Enami, S. and Sakamoto, Y.: OH-radical oxidation of surface-active cis-pinonic acid at the air–water interface, J. Phys. Chem. A., 120, 3578-3587, 2016b.
Henry's law constants were calcualted with HenryWin (EPI Suite v4.11) Website: https://www.epa.gov/tsca-screening-tools/epi-suitetm-estimation-program-interface, last access Jun 20th 2023, last
Ervens, B.: Modeling the processing of aerosol and trace gases in clouds and fogs, Chemical reviews, 115, 4157-4198, 2015.
Ervens, B., Turpin, B. J., and Weber, R. J.: Secondary organic aerosol formation in cloud droplets and aqueous particles (aqSOA): a review of laboratory, field and model studies, Atmos. Chem. Phys., 11, 11069-11102, 10.5194/acp-11-11069-2011, 2011.
Ervens, B., Sorooshian, A., Aldhaif, A. M., Shingler, T., Crosbie, E., Ziemba, L., Campuzano-Jost, P., Jimenez, J. L., and Wisthaler, A.: Is there an aerosol signature of chemical cloud processing?, Atmos. Chem. Phys., 18, 16099-16119, https://doi.org/10.5194/acp-18-16099-2018, 2018.
Fuzzi, S., Baltensperger, U., Carslaw, K., Decesari, S., Denier van der Gon, H., Facchini, M. C., Fowler, D., Koren, I., Langford, B., Lohmann, U., Nemitz, E., Pandis, S., Riipinen, I., Rudich, Y., Schaap, M., Slowik, J. G., Spracklen, D. V., Vignati, E., Wild, M., Williams, M., and Gilardoni, S.: Particulate matter, air quality and climate: lessons learned and future needs, Atmos. Chem. Phys., 15, 8217-8299, 10.5194/acp-15-8217-2015, 2015.
Gentner, D., Ormeño, E., Fares, S., Ford, T., Weber, R., Park, J.-H., Brioude, J., Angevine, W., Karlik, J., and Goldstein, A.: Emissions of terpenoids, benzenoids, and other biogenic gas-phase organic compounds from agricultural crops and their potential implications for air quality, Atmos. Chem. Phys., 14, 5393-5413, 2014.
Ghaffari, Z., Rahimmalek, M., and Sabzalian, M. R.: Variation in the primary and secondary metabolites derived from the isoprenoid pathway in the Perovskia species in response to different wavelengths generated by light emitting diodes (LEDs), Ind. Crops Prod., 140, 111592, https://doi.org/10.1016/j.indcrop.2019.111592, 2019.
Gierczak, T., Bernard, F., Papanastasiou, D. K., and Burkholder, J. B.: Atmospheric Chemistry of c-C5HF7 and c-C5F8: Temperature-Dependent OH Reaction Rate Coefficients, Degradation Products, Infrared Spectra, and Global Warming Potentials, J. Phys. Chem. A., 125, 1050-1061, 10.1021/acs.jpca.0c10561, 2021.
Gligorovski, S., Strekowski, R., Barbati, S., and Vione, D.: Environmental Implications of Hydroxyl Radicals (•OH), Chemical Reviews, 115, 13051-13092, 10.1021/cr500310b, 2015.
Gomez, M. E., Lin, Y., Guo, S., and Zhang, R.: Heterogeneous Chemistry of Glyoxal on Acidic Solutions. An Oligomerization Pathway for Secondary Organic Aerosol Formation, J. Phys. Chem. A., 119, 4457-4463, 10.1021/jp509916r, 2015.
Graedel, T.: Terpenoids in the atmosphere, Rev. Geophys., 17, 937-947, 1979.
Griffin, R. J., Cocker III, D. R., Seinfeld, J. H., and Dabdub, D.: Estimate of global atmospheric organic aerosol from oxidation of biogenic hydrocarbons, Geophys. Res. Lett., 26, 2721-2724, 1999.
Guenther, A. B., Jiang, X., Heald, C. L., Sakulyanontvittaya, T., Duhl, T., Emmons, L. K., and Wang, X.: The Model of Emissions of Gases and Aerosols from Nature version 2.1 (MEGAN2.1): an extended and updated framework for modeling biogenic emissions, Geosci. Model Dev., 5, 1471-1492, 10.5194/gmd-5-1471-2012, 2012.
Hallquist, M., Wenger, J. C., Baltensperger, U., Rudich, Y., Simpson, D., Claeys, M., Dommen, J., Donahue, N., George, C., and Goldstein, A.: The formation, properties and impact of secondary organic aerosol: current and emerging issues, Atmos. Chem. Phys., 9, 5155-5236, 2009.
Hatch, L. E., Jen, C. N., Kreisberg, N. M., Selimovic, V., Yokelson, R. J., Stamatis, C., York, R. A., Foster, D., Stephens, S. L., Goldstein, A. H., and Barsanti, K. C.: Highly Speciated Measurements of Terpenoids Emitted from Laboratory and Mixed-Conifer Forest Prescribed Fires, Environ. Sci. Technol., 53, 9418-9428, 10.1021/acs.est.9b02612, 2019.
Herrmann, H., Schaefer, T., Tilgner, A., Styler, S. A., Weller, C., Teich, M., and Otto, T.: Tropospheric Aqueous-Phase Chemistry: Kinetics, Mechanisms, and Its Coupling to a Changing Gas Phase, Chem. Rev., 115, 4259-4334, 10.1021/cr500447k, 2015.

https://doi.org/10.5194/egusphere-2026-1788
Preprint. Discussion started: 18 May 2026

Hodzic, A., Kasibhatla, P. S., Jo, D. S., Cappa, C. D., Jimenez, J. L., Madronich, S., and Park, R. J.: Rethinking the global secondary organic aerosol (SOA) budget: stronger production, faster removal, shorter lifetime, Atmos. Chem. Phys., 16, 7917-7941, 10.5194/acp-16-7917-2016, 2016.

Hoffmann, E. H., Tilgner, A., Wolke, R., Böge, O., Walter, A., and Herrmann, H.: Oxidation of substituted aromatic hydrocarbons in the tropospheric aqueous phase: kinetic mechanism development and modelling, Phys. Chem. Chem. Phys., 20, 10960-10977, 10.1039/C7CP08576A, 2018.

Huang, Y., Barraza, K. M., Kenseth, C. M., Zhao, R., Wang, C., Beauchamp, J. L., and Seinfeld, J. H.: Probing the OH Oxidation of Pinonic Acid at the Air–Water Interface Using Field-Induced Droplet Ionization Mass Spectrometry (FIDI-MS), J. Phys. Chem. A, 122, 6445-6456, 10.1021/acs.jpca.8b05353, 2018.

ICCP: AR6 Synthesis Report Climate Change 2023, Intergovernmental Panel on Climate Change, 2023.

Jain, P., Witkowski, B., Błaziak, A., and Gierczak, T.: Efficient Formation of Secondary Organic Aerosols from the Aqueous Oxidation of Terpenoic 1,2-Diols by OH, Environ. Sci. Technol., 58, 22089-22103, 10.1021/acs.est.4c06347, 2024.

Javelle, T., Righezza, M., and Danger, G.: Identify low mass volatile organic compounds from cometary ice analogs using gas chromatography coupled to an Orbitrap mass spectrometer associated to electron and chemical ionizations, J. Chromatogr. A., 1652, 462343, 2021.

Jimenez, J. L., Canagaratna, M. R., Donahue, N. M., Prevot, A. S. H., Zhang, Q., Kroll, J. H., DeCarlo, P. F., Allan, J. D., Coe, H., Ng, N. L., Aiken, A. C., Docherty, K. S., Ulbrich, I. M., Grieshop, A. P., Robinson, A. L., Duplissy, J., Smith, J. D., Wilson, K. R., Lanz, V. A., Hueglin, C., Sun, Y. L., Tian, J., Laaksonen, A., Raatikainen, T., Rautiainen, J., Vaattovaara, P., Ehn, M., Kulmala, M., Tomlinson, J. M., Collins, D. R., Cubison, M. J., Dunlea, J., Huffman, J. A., Onasch, T. B., Alfarra, M. R., Williams, P. I., Bower, K., Kondo, Y., Schneider, J., Drewnick, F., Borrmann, S., Weimer, S., Demerjian, K., Salcedo, D., Cottrell, L., Griffin, R., Takami, A., Miyoshi, T., Hatakeyama, S., Shimono, A., Sun, J. Y., Zhang, Y. M., Dzepina, K., Kimmel, J. R., Sueper, D., Jayne, J. T., Herndon, S. C., Trimborn, A. M., Williams, L. R., Wood, E. C., Middlebrook, A. M., Kolb, C. E., Baltensperger, U., and Worsnop, D. R.: Evolution of Organic Aerosols in the Atmosphere, Science, 326, 1525-1529, 2009.

Jo, D. S., Nault, B. A., Tilmes, S., Gettelman, A., McCluskey, C. S., Hodzic, A., Henze, D. K., Nawaz, M. O., Fung, K. M., and Jimenez, J. L.: Global Health and Climate Effects of Organic Aerosols from Different Sources, Environ. Sci. Technol., 57, 13793-13807, 10.1021/acs.est.3c02823, 2023.

Kamatou, G. P. P., Vermaak, I., Viljoen, A. M., and Lawrence, B. M.: Menthol: A simple monoterpene with remarkable biological properties, Phytochemistry, 96, 15-25, https://doi.org/10.1016/j.phytochem.2013.08.005, 2013.

Kamens, R. M. and Jaoui, M.: Modeling aerosol formation from alpha-pinene plus NO_x in the presence of natural sunlight using gas-phase kinetics and gas-particle partitioning theory, Environ. Sci. Technol., 35, 1394-1405, 10.1021/es001626s, 2001.

Kanakidou, M., Seinfeld, J. H., Pandis, S. N., Barnes, I., Dentener, F. J., Facchini, M. C., Van Dingenen, R., Ervens, B., Nenes, A., Nielsen, C. J., Swietlicki, E., Putaud, J. P., Balkanski, Y., Fuzzi, S., Horth, J., Moortgat, G. K., Winterhalter, R., Myhre, C. E. L., Tsigaridis, K., Vignati, E., Stephanou, E. G., and Wilson, J.: Organic aerosol and global climate modelling: a review, Atmos. Chem. Phys., 5, 1053-1123, 10.5194/acp-5-1053-2005, 2005.

Keating, L., Harris, H. H., and Chickos, J. S.: Vapor pressures and vaporization enthalpy of (−) α-bisabolol and (dl) menthol by correlation gas chromatography, J. Chem. Thermodyn., 107, 18-25, https://doi.org/10.1016/j.jct.2016.11.027, 2017.

Kelly, J. M., Doherty, R. M., O'Connor, F. M., and Mann, G. W.: The impact of biogenic, anthropogenic, and biomass burning volatile organic compound emissions on regional and seasonal variations in secondary organic aerosol, Atmos. Chem. Phys., 18, 7393-7422, 2018.

Kenseth, C. M., Hafeman, N. J., Huang, Y., Dalleska, N. F., Stoltz, B. M., and Seinfeld, J. H.: Synthesis of Carboxylic Acid and Dimer Ester Surrogates to Constrain the Abundance and Distribution of Molecular Products in α-Pinene and β-Pinene Secondary Organic Aerosol, Environ. Sci. Technol., 54, 12829-12839, 10.1021/acs.est.0c01566, 2020.

Khalaj, F., Gu, S., Mehra, A., Williams, L. R., Krechmer, J., Lambe, A., Perraud, V., and Faiola, C. L.: Aerosol chemistry of oxygenated terpenes in simple and complex chemical systems, Aerosol Sci. Tech., 59, 470-486, 10.1080/02786826.2024.2427283, 2025.

https://doi.org/10.5194/egusphere-2026-1788
Preprint. Discussion started: 18 May 2026

Kopinke, F.-D. and Georgi, A.: What Controls Selectivity of Hydroxyl Radicals in Aqueous Solution? Indications for a Cage Effect, J. Phys. Chem. A, 121, 7947-7955, https://doi.org/10.1021/acs.jpca.7b05782, 2017.

Kourtchev, I., Fuller, S. J., Giorio, C., Healy, R. M., Wilson, E., O'Connor, I., Wenger, J. C., McLeod, M., Aalto, J., Ruuskanen, T. M., Maenhaut, W., Jones, R., Venables, D. S., Sodeau, J. R., Kulmala, M., and Kalberer, M.: Molecular composition of biogenic secondary organic aerosols using ultrahigh-resolution mass spectrometry: comparing laboratory and field studies, Atmos. Chem. Phys., 14, 2155-2167, 10.5194/acp-14-2155-2014, 2014.

Kuang, X. M., Gonzalez, D. H., Scott, J. A., Vu, K., Hasson, A., Charbouillot, T., Hawkins, L., and Paulson, S. E.: Cloud Water Chemistry Associated with Urban Aerosols: Rapid Hydroxyl Radical Formation, Soluble Metals, Fe(II), Fe(III), and Quinones, ACS Earth Space Chem., 4, 67-76, 10.1021/acsearthspacechem.9b00243, 2020a.

Kuang, Y., He, Y., Xu, W., Yuan, B., Zhang, G., Ma, Z., Wu, C., Wang, C., Wang, S., Zhang, S., Tao, J., Ma, N., Su, H., Cheng, Y., Shao, M., and Sun, Y.: Photochemical Aqueous-Phase Reactions Induce Rapid Daytime Formation of Oxygenated Organic Aerosol on the North China Plain, Environ. Sci. Technol., 54, 3849-3860, 10.1021/acs.est.9b06836, 2020b.

Kwok, E. S. C. and Atkinson, R.: Estimation of hydroxyl radical reaction rate constants for gas-phase organic compounds using a structure-reactivity relationship: An update, Atmos. Environ., 29, 1685-1695, https://doi.org/10.1016/1352-2310(95)00069-B, 1995.

Lai, D., Bai, Y., Zhang, Z., So, P. K., Li, Y. J., Tse, Y. L. S., Yeung, Y. Y., Schaefer, T., Herrmann, H., Yu, J. Z., Wang, Y., and Chan, M. N.: Rapid aqueous-phase oxidation of an α-pinene-derived organosulfate by hydroxyl radicals: a potential source of some unclassified oxygenated and small organosulfates in the atmosphere, Atmos. Chem. Phys., 25, 12569-12584, 10.5194/acp-25-12569-2025, 2025.

Lee, A., Goldstein, A. H., Kroll, J. H., Ng, N. L., Varutbangkul, V., Flagan, R. C., and Seinfeld, J. H.: Gas-phase products and secondary aerosol yields from the photooxidation of 16 different terpenes, J. Geophys. Res. Atmos., 111, https://doi.org/10.1029/2006JD007050, 2006.

Leviss, D. H., Ry, D. A. V., and Hinrichs, R. Z.: Multiphase Ozonolysis of Aqueous α-Terpineol, Environ. Sci. Technol, 10.1021/acs.est.6b03612, 2016.

Li, F., Tang, S., Tsona, N. T., and Du, L.: Kinetics and mechanism of OH-induced α-terpineol oxidation in the atmospheric aqueous phase, Atmos. Environ., 237, 117650, 2020.

Lim, Y. B., Tan, Y., Perri, M. J., Seitzinger, S. P., and Turpin, B. J.: Aqueous chemistry and its role in secondary organic aerosol (SOA) formation, Atmos. Chem. Phys., 10, 10521-10539, 10.5194/acp-10-10521-2010, 2010.

Liu, D., Zhang, Y., Zhong, S., Chen, S., Xie, Q., Zhang, D., Zhang, Q., Hu, W., Deng, J., Wu, L., Ma, C., Tong, H., and Fu, P.: Large differences of highly oxygenated organic molecules (HOMs) and low-volatile species in secondary organic aerosols (SOAs) formed from ozonolysis of β-pinene and limonene, Atmos. Chem. Phys., 23, 8383-8402, 10.5194/acp-23-8383-2023, 2023.

Mahilang, M., Deb, M. K., and Pervez, S.: Biogenic secondary organic aerosols: A review on formation mechanism, analytical challenges and environmental impacts, Chemosphere, 262, 127771, https://doi.org/10.1016/j.chemosphere.2020.127771, 2021.

McNeill, V. F.: Aqueous organic chemistry in the atmosphere: Sources and chemical processing of organic aerosols, Environ. Sci. Technol., 49, 1237-1244, 10.1021/ES5043707/ASSET/IMAGES/LARGE/ES-2014-043707_0003.JPEG, 2015.

Mehra, A., Krechmer, J. E., Lambe, A., Sarkar, C., Williams, L., Khalaj, F., Guenther, A., Jayne, J., Coe, H., and Worsnop, D.: Oligomer and highly oxygenated organic molecule formation from oxidation of oxygenated monoterpenes emitted by California sage plants, Atmos. Chem. Phys., 20, 10953-10965, 2020.

Mekic, M., Liu, J., Zhou, W., Loisel, G., Cai, J., He, T., Jiang, B., Yu, Z., Lazarou, Y. G., Li, X., Brigante, M., Vione, D., and Gligorovski, S.: Formation of highly oxygenated multifunctional compounds from cross-reactions of carbonyl compounds in the atmospheric aqueous phase, Atmos. Environ., 219, 117046, https://doi.org/10.1016/j.atmosenv.2019.117046, 2019.

Messina, P., Lathière, J., Sindelarova, K., Vuichard, N., Granier, C., Ghattas, J., Cozic, A., and Hauglustaine, D. A.: Global biogenic volatile organic compound emissions in the ORCHIDEE and MEGAN models and sensitivity to key parameters, Atmos. Chem. Phys., 16, 14169-14202, https://doi.org/10.5194/acp-16-14169-2016, 2016.

https://doi.org/10.5194/egusphere-2026-1788
Preprint. Discussion started: 18 May 2026

Mitroka, S., Zimmeck, S., Troya, D., and Tanko, J. M.: How Solvent Modulates Hydroxyl Radical Reactivity in Hydrogen Atom Abstractions, J. Am. Chem. Soc., 132, 2907-2913, 10.1021/ja903856t, 2010.

Odum, J. R., Hoffmann, T., Bowman, F., Collins, D., Flagan, R. C., and Seinfeld, J. H.: Gas/Particle Partitioning and Secondary Organic Aerosol Yields, Environ. Sci. Technol., 30, 2580-2585, 10.1021/es950943+, 1996.

Ormeño, E., Gentner, D. R., Fares, S., Karlik, J., Park, J. H., and Goldstein, A. H.: Sesquiterpenoid emissions from agricultural crops: correlations to monoterpenoid emissions and leaf terpene content, Environ. Sci. Technol., 44, 3758-3764, 2010.

Otto, S. and Engberts, J. B. F. N.: Hydrophobic interactions and chemical reactivity, Org. Biomol. Chem., 1, 2809-2820, https://doi.org/10.1039/B305672D, 2003.

Otto, T., Schaefer, T., and Herrmann, H.: Aqueous-Phase Oxidation of Terpene-Derived Acids by Atmospherically Relevant Radicals, J. Phys. Chem. A., 122, 9233-9241, 10.1021/acs.jpca.8b08922, 2018.

Paglione, M., Gilardoni, S., Rinaldi, M., Decesari, S., Zanca, N., Sandrini, S., Giulianelli, L., Bacco, D., Ferrari, S., Poluzzi, V., Scotto, F., Trentini, A., Poulain, L., Herrmann, H., Wiedensohler, A., Canonaco, F., Prévôt, A. S. H., Massoli, P., Carbone, C., Facchini, M. C., and Fuzzi, S.: The impact of biomass burning and aqueous-phase processing on air quality: a multi-year source apportionment study in the Po Valley, Italy, Atmos. Chem. Phys., 20, 1233-1254, 10.5194/acp-20-1233-2020, 2020.

Pankow, J. F.: An absorption model of the gas/aerosol partitioning involved in the formation of secondary organic aerosol, Atmos. Environ., 28, 189-193, https://doi.org/10.1016/1352-2310(94)90094-9, 1994.

Paulson, S. E., Gallimore, P. J., Kuang, X. M., Chen, J. R., Kalberer, M., and Gonzalez, D. H.: A light-driven burst of hydroxyl radicals dominates oxidation chemistry in newly activated cloud droplets, Sci. Adv., 5, eaav7689, doi:10.1126/sciadv.aav7689, 2019.

Price, P., Bottorff, B., Jenkins, J., Brune, W. H., and Stevens, P. S.: Re-assessing hydroxyl radical chemistry in the atmosphere: Instrument interferences may explain previous measurement discrepancies, Commun. Earth Environ., 6, 325, 10.1038/s43247-025-02308-y, 2025.

Prisle, N. L.: A predictive thermodynamic framework of cloud droplet activation for chemically unresolved aerosol mixtures, including surface tension, non-ideality, and bulk–surface partitioning, Atmos. Chem. Phys., 21, 16387-16411, 2021.

Puchkov, S., Buneeva, E., and Perkel', A.: Composition and stability of peroxide products of liquid-phase cyclohexanol oxidation, Kinet. Catal., 46, 340-343, 2005.

Puchkov, S., Moskvitina, E., Nepomnyashchikh, Y. V., and Perkel', A.: Features of the kinetics of the liquid-phase oxidation of cyclohexanol, Russ. J. Phys. Chem. A., 87, 737-741, 2013.

Russell, G. A.: Deuterium-isotope effects in the autoxidation of aralkyl hydrocarbons. mechanism of the interaction of peroxy radicals1, J. Am. Chem. Soc., 79, 3871-3877, 1957.

Sarang, K., Otto, T., Rudzinski, K., Schaefer, T., Grgić, I., Nestorowicz, K., Herrmann, H., and Szmigielski, R.: Reaction Kinetics of Green Leaf Volatiles with Sulfate, Hydroxyl, and Nitrate Radicals in Tropospheric Aqueous Phase, Environ. Sci. Technol., 55, 13666-13676, 10.1021/acs.est.1c03276, 2021.

Scheres Firak, D., Schaefer, T., Senff, P., Cheng, P., Sarakha, M., Brigante, M., Mailhot, G., and Herrmann, H.: Fenton-like Reactions in Acidic Environments: New Mechanistic Insights and Implications to Atmospheric Particle-Phase Chemistry, ACS ES&T Air, 2, 1315-1325, 10.1021/acsestair.5c00077, 2025.

Shrivastava, M., Cappa, C. D., Fan, J., Goldstein, A. H., Guenther, A. B., Jimenez, J. L., Kuang, C., Laskin, A., Martin, S. T., and Ng, N. L.: Recent advances in understanding secondary organic aerosol: Implications for global climate forcing, Rev. Geophys., 55, 509-559, 2017a.

Shrivastava, M., Cappa, C. D., Fan, J., Goldstein, A. H., Guenther, A. B., Jimenez, J. L., Kuang, C., Laskin, A., Martin, S. T., Ng, N. L., Petaja, T., Pierce, J. R., Rasch, P. J., Roldin, P., Seinfeld, J. H., Shilling, J., Smith, J. N., Thornton, J. A., Volkamer, R., Wang, J., Worsnop, D. R., Zaveri, R. A., Zelenyuk, A., and Zhang, Q.: Recent advances in understanding secondary organic aerosol: Implications for global climate forcing, Rev. Geophys., 55, 509-559, https://doi.org/10.1002/2016RG000540, 2017b.

Sindelarova, K., Markova, J., Simpson, D., Huszar, P., Karlicky, J., Darras, S., and Granier, C.: High-resolution biogenic global emission inventory for the time period 2000–2019 for air quality modelling, Earth Syst. Sci. Data, 14, 251-270, 10.5194/essd-14-251-2022, 2022.

https://doi.org/10.5194/egusphere-2026-1788
Preprint. Discussion started: 18 May 2026

Sporre, M. K., Blichner, S. M., Schrödner, R., Karset, I. H. H., Berntsen, T. K., van Noije, T., Bergman, T., O'Donnell, D., and Makkonen, R.: Large difference in aerosol radiative effects from BVOC-SOA treatment in three Earth system models, Atmos. Chem. Phys., 20, 8953-8973, 10.5194/acp-20-8953-2020, 2020.

Su, H., Cheng, Y., and Pöschl, U.: New Multiphase Chemical Processes Influencing Atmospheric Aerosols, Air Quality, and Climate in the Anthropocene, Acc. Chem. Res., 53, 2034-2043, 10.1021/acs.accounts.0c00246, 2020.

Sullivan, A. P., Hodas, N., Turpin, B. J., Skog, K., Keutsch, F. N., Gilardoni, S., Paglione, M., Rinaldi, M., Decesari, S., Facchini, M. C., Poulain, L., Herrmann, H., Wiedensohler, A., Nemitz, E., Twigg, M. M., and Collett Jr, J. L.: Evidence for ambient dark aqueous SOA formation in the Po Valley, Italy, Atmos. Chem. Phys., 16, 8095-8108, 10.5194/acp-16-8095-2016, 2016.

Sun, Y. L., Zhang, Q., Anastasio, C., and Sun, J.: Insights into secondary organic aerosol formed via aqueous-phase reactions of phenolic compounds based on high resolution mass spectrometry, Atmos. Chem. Phys., 10, 4809-4822, 10.5194/acp-10-4809-2010, 2010.

Tsigaridis, K. and Kanakidou, M.: The Present and Future of Secondary Organic Aerosol Direct Forcing on Climate, Curr. Clim. Change Rep., 4, 84-98, 10.1007/s40641-018-0092-3, 2018.

Tsui, W. G., Woo, J. L., and McNeill, V. F.: Impact of Aerosol-Cloud Cycling on Aqueous Secondary Organic Aerosol Formation, Atmosphere, 10, 666, 2019.

Valorso, R., Aumont, B., Camredon, M., Raventos-Duran, T., Mouchel-Vallon, C., Ng, N. L., Seinfeld, J. H., Lee-Taylor, J., and Madronich, S.: Explicit modelling of SOA formation from α-pinene photooxidation: sensitivity to vapour pressure estimation, Atmos. Chem. Phys., 11, 6895-6910, 10.5194/acp-11-6895-2011, 2011.

Wang, H., Liu, X., Wu, C., and Lin, G.: Regional to global distributions, trends, and drivers of biogenic volatile organic compound emission from 2001 to 2020, Atmos. Chem. Phys., 24, 3309-3328, 10.5194/acp-24-3309-2024, 2024.

Wei, Y., Wang, Y., Di, Q., Choirat, C., Wang, Y., Koutrakis, P., Zanobetti, A., Dominici, F., and Schwartz, J. D.: Short term exposure to fine particulate matter and hospital admission risks and costs in the Medicare population: time stratified, case crossover study, BMJ, 367, l6258, 10.1136/bmj.l6258, 2019.

Witkowski, B., Al-sharafi, M., and Gierczak, T.: Ozonolysis of β-Caryophyllonic and Limononic Acids in the Aqueous Phase: Kinetics, Product Yield, and Mechanism, Environ. Sci. Technol., 53, 8823-8832, 10.1021/acs.est.9b02471, 2019.

Witkowski, B., Jain, P., Wileńska, B., and Gierczak, T.: Temperature-dependent aqueous OH kinetics of C 2–C 10 linear and terpenoid alcohols and diols: new rate coefficients, structure–activity relationship, and atmospheric lifetimes, Atmospheric Chemistry and Physics, 24, 663-688, 2024a.

Witkowski, B., Jain, P., Wileńska, B., and Gierczak, T.: Temperature-dependent aqueous OH kinetics of C_2–C_{10} linear and terpenoid alcohols and diols: new rate coefficients, structure–activity relationship, and atmospheric lifetimes, Atmos. Chem. Phys., 24, 663-688, 10.5194/acp-24-663-2024, 2024b.

Xu, L., Du, L., Tsona, N. T., and Ge, M.: Anthropogenic Effects on Biogenic Secondary Organic Aerosol Formation, Adv. Atmos. Sci., 38, 1053-1084, 10.1007/s00376-020-0284-3, 2021.

Yang, W., Cao, J., Wu, Y., Kong, F., and Li, L.: Review on plant terpenoid emissions worldwide and in China, Sci. Total Environ., 787, 147454, 2021.

Yasmeen, F., Szmigielski, R., Vermeylen, R., Gómez-González, Y., Surratt, J. D., Chan, A. W. H., Seinfeld, J. H., Maenhaut, W., and Claeys, M.: Mass spectrometric characterization of isomeric terpenoic acids from the oxidation of α-pinene, β-pinene, d-limonene, and Δ3-carene in fine forest aerosol, J. Mass Spectrom., 46, 425-442, https://doi.org/10.1002/jms.1911, 2011.

Yassaa, N., Youcef Meklati, B., and Cecinato, A.: Evaluation of monoterpenic biogenic volatile organic compounds in ambient air around Eucalyptus globulus, Pinus halepensis and Cedrus atlantica trees growing in Algiers city area by chiral and achiral capillary gas chromatography, Atmos. Environ., 34, 2809-2816, https://doi.org/10.1016/S1352-2310(99)00436-7, 2000.

Ye, P., Zhao, Y., Chuang, W. K., Robinson, A. L., and Donahue, N. M.: Secondary organic aerosol production from pinanediol, a semi-volatile surrogate for first-generation oxidation products of monoterpenes, Atmos. Chem. Phys., 18, 6171-6186, 10.5194/ACP-18-6171-2018, 2018.

https://doi.org/10.5194/egusphere-2026-1788
Preprint. Discussion started: 18 May 2026

Zhang, Q., Alfarra, M. R., Worsnop, D. R., Allan, J. D., Coe, H., Canagaratna, M. R., and Jimenez, J. L.: Deconvolution and Quantification of Hydrocarbon-like and Oxygenated Organic Aerosols Based on Aerosol Mass Spectrometry, Environ. Sci. Technol., 39, 4938-4952, 10.1021/es048568l, 2005.

Zhang, X., McVay, R. C., Huang, D. D., Dalleska, N. F., Aumont, B., Flagan, R. C., and Seinfeld, J. H.: Formation and evolution of molecular products in α-pinene secondary organic aerosol, Proc. Natl. Acad. Sci. U. S. A., 112, 14168-14173, doi:10.1073/pnas.1517742112, 2015.

Zheng, Y., Chen, Q., Cheng, X., Mohr, C., Cai, J., Huang, W., Shrivastava, M., Ye, P., Fu, P., Shi, X., Ge, Y., Liao, K., Miao, R., Qiu, X., Koenig, T. K., and Chen, S.: Precursors and Pathways Leading to Enhanced Secondary Organic Aerosol Formation during Severe Haze Episodes, Environ. Sci. Technol., 55, 15680-15693, 10.1021/acs.est.1c04255, 2021.

Zhu, Y., Tilgner, A., Hoffmann, E. H., Herrmann, H., Kawamura, K., Yang, L., Xue, L., and Wang, W.: Multiphase MCM–CAPRAM modeling of the formation and processing of secondary aerosol constituents observed during the Mt. Tai summer campaign in 2014, Atmos. Chem. Phys., 20, 6725-6747, 2020.

Zuzarte, M. and Salgueiro, L.: Essential oils chemistry, Bioactive essential oils and cancer, 19-61, 2015.